Microbial Pathogenesis 201 (2025) 107373

Contents lists available at ScienceDirect

Microbial Pathogenesis

journal homepage: www.elsevier.com/locate/micpath

Combinatory effects of chlorhexidine and azithromycin: Implications for therapeutic potential and mechanistic insights

Sinem Tunçer Çağlayan

Vocational School of Health Services, Department of Medical Services and Techniques, Bilecik Şeyh Edebali University, 11100, Bilecik, Türkiye

ARTICLE INFO

Keywords:
Chlorhexidine
Azithromycin
Pseudomonas aeruginosa
Wound
Streptococcus mutans
Cancer cell toxicity

ABSTRACT

The use of drug combinations to re-sensitize resistant strains is a promising strategy to overcome the stagnation in the drug discovery pipeline. Here, the results demonstrate that the combined application of the broad-spectrum bisbiguanide antiseptic chlorhexidine (CHX) and the macrolide antibiotic azithromycin (AZM) significantly inhibits the growth of the *Pseudomonas aeruginosa* strain PAO1 (isolated from a wound) compared to the individual effects of each agent. Specifically, 1.5 μg/mL CHX caused 11.4 ± 4 % growth inhibition and 2 μg/mL AZM resulted in 14 ± 4.5 % inhibition; however, the combination of 1.5 μg/mL CHX and 2 μg/mL AZM achieved 58 ± 6 % inhibition, significantly exceeding the sum of their individual effects. Furthermore, the AZM and CHX combination reduced bacterial viability in biofilms. *P. aeruginosa* is a common pathogen in wounds, particularly chronic wounds, where it delays the healing process. An *in vitro* wound infection model further demonstrated that CHX and AZM combination reduced bacterial density and activity in a serum-supported collagen matrix. This combination was found to be effective not only against the Gram-negative *P. aeruginosa* but also against the Gram-positive *Streptococcus mutans*.

To explain the observed combinatory inhibition effect mechanistically, Fourier Transform Infrared Spectroscopy (FTIR) was employed for the first time in the literature. The results reveal that CHX increases the cellular accumulation of AZM. Changes in the membrane lipid composition of the bacteria additionally suggest a mechanism for enhanced antibiotic accumulation in the presence of CHX.

These findings suggest that the role of CHX as a potential partner in different syncretic combinations calls for comprehensive exploration in antibiotic resistant bacterial infections.

1. Introduction

Despite intensive drug discovery efforts, the chemical, biological, and pharmacological characteristics required for effective antibiotics have resulted in a lack of new antibiotic classes for decades. Additionally, the discovery of new antibiotics cannot keep pace with the rate of antimicrobial resistance (AMR) [1,2]. In this context, the use of combinations to re-sensitize resistant strains should be considered a promising strategy [3].

Although comprehensive studies and publications have extensively explored the combined effects of different antibiotic combinations, there has been a lack of systematic investigation into the effects of using antibiotics in conjunction with biocides or antiseptics as antimicrobials [4]. Biocides have been widely used for decades to control bacteria and are included in various products, including disinfectants, preservatives, pesticides, cosmetics, and antiseptics [5]. Chlorhexidine (CHX; $C_{22}H_{30}Cl_2N_{10}$), a broad-spectrum bisbiguanide antiseptic, disinfectant, and preservative, is an effective antimicrobial agent against both aerobic and anaerobic bacteria. Considered “safe”, it has been used in applications such as hand washing for both adults and children, pre-surgical skin preparation, washing of equipment such as catheters, vaginal antisepsis, treatment of gum inflammation, and body washing in intensive care units [6,7]. CHX typically functions as a bacteriostatic agent at low concentrations and as a bactericidal agent at high concentrations. It has been reported that CHX enters the double membrane layer of bacteria at sites where divalent cations on the outer surface are displaced, disrupting the cell membrane by creating gaps between adjacent lipid groups, including lipopolysaccharides (LPS) [8]. Additionally, CHX is adsorbed onto phosphate-containing protein components in the bacterial cell wall [9]. At low concentrations, CHX disrupts cytoplasmic membrane integrity and the activity of membrane-bound enzymes, while at higher concentrations, it causes membrane damage, cytoplasmic leakage, and the coagulation and precipitation of intracellular components such as proteins and nucleic acids [10].

E-mail address: sinem.tuncer@bilecik.edu.tr.

https://doi.org/10.1016/j.micpath.2025.107373
Received 30 August 2024; Received in revised form 28 January 2025; Accepted 10 February 2025
Available online 10 February 2025

Azithromycin (AZM; $C_{38}H_{72}N_2O_{12}$), a second-generation, broad-spectrum, semi-synthetic antibiotic, has been employed since the 1980s to treat respiratory, urogenital, dermal, and numerous other bacterial infections. Additionally, it acts as an immunomodulator in chronic inflammatory disorders [11]. Macrolides exert their bacteriostatic effects by inhibiting bacterial protein synthesis, thereby preventing bacterial growth. They achieve this through reversible interaction with 23S rRNA, inhibiting bacterial protein translation by blocking the peptide exit tunnel of the 50S ribosomal subunit. Consequently, they impede the progression of the nascent chain, leading to premature dissociation of incomplete peptide chains, a phenomenon known as "peptidyl-tRNA drop," which depletes the intracellular pools of aminoacyl-tRNA available for protein synthesis [12]. Similar to other antibiotics, suboptimal use of AZM (incorrect dosage and/or treatment duration) is considered a primary reason for the development of resistant bacteria [13,14]. Here, the impact of the combined application of AZM and CHX on the *Pseudomonas aeruginosa* strain PAO1, isolated from a wound and devoid of mutations in the 23S rRNA gene, was examined [15].

As a Gram-negative opportunistic pathogen, *P. aeruginosa* (PA) is among the most common bacterial species observed in wounds, particularly chronic wounds. The microenvironment of a wound is ideal for biological load and typically harbors numerous bacterial species. It is known that bacterial proliferation in wounds contributes to infection and delays wound healing. Immunocompromised patients, those with vascular diseases, and those with comorbidities such as diabetes are particularly susceptible to PA infections [16]. Wounds where PA is detected tend to be larger and longer lasting, with PA exacerbating faster deterioration and leading to a higher incidence of sepsis. Similarly, the presence of PA in leg ulcers is associated with larger wound sizes, delayed healing, and a higher rate of skin graft failure. Due to limited treatment options and the potential for antibiotic resistance development, PA is recognized as a priority pathogen by the World Health Organization (WHO) for the development of new therapies [16]. AZM has modest activity against PA and is not considered a highly effective antibiotic against this pathogen [17]: the minimum inhibitory concentration (MIC) values are quite high (8–512 μg/mL and above), and long-term low-dose AZM therapy [12] carries an increased risk of resistance development [18]. The results of this study demonstrate that the combined application of CHX and AZM exhibits a significantly stronger inhibitory effect on the growth of the PA strain PAO1 compared to each agent alone, similar to what we have observed previously for *Escherichia coli* [19]. Additionally, this combination cumulatively reduces bacterial viability in the PAO1 biofilm. Moreover, *in vitro* wound model studies show that the combined application reduces bacterial density and activity in the collagen matrix. It is found that CHX increases the bacterial accumulation of AZM, which mechanistically explains the observed biological effects.

2. Materials and methods

2.1. Bacterial growth and treatments for minimum inhibitory concentration (MIC) determination

Pseudomonas aeruginosa (PAO1) and *Streptococcus mutans* Clarke (ATCC 35668) were cultured in tryptic soy broth (TSB; Cat no: 1224; Condalab, Spain) or on plates (TSA) containing 1.5 % (w/v) agar (Cat no: 1802, Condalab) in TSB at 37 °C as previously described [20,21]. CHX (Chlorhexidine diacetate salt, $C_{26}H_{38}Cl_2N_{10}O_4$; Cat no: sc-252569B; Santa Cruz, California, USA) primary stocks were prepared at 19 mg/mL in sterile dH_2O, as specified by the manufacturer. AZM (Azithromycin dihydrate, $C_{38}H_{76}N_2O_{14}$; Cat no: PHR1088-1G; Sigma, St. Louis, Missouri, USA) stocks were prepared at 100 mg/mL in cell culture grade DMSO (Cat no: sc-358801, Santa Cruz) and stored at −80 °C protected from light. Working concentrations of CHX and AZM at 1 mg/mL were prepared in sterile dH_2O and aliquoted for storage at −20 °C in the dark. Bacteria cultured overnight were diluted the following day to 10^3 CFU (Colony-Forming Units)/mL in TSB. The microdilution method was used to determine the minimum inhibitory concentrations (MICs) of AZM and CHX against *Pseudomonas aeruginosa* (PAO1) using 96-well plates (Cat. No.: 701001; Nest Scientific, New Jersey, USA), as described elsewhere [22]. After 24 h of incubation at 37 °C with shaking, changes in culture turbidity were assessed by measuring optical density at 600 nm using a microplate reader (Multiskan FC, Thermo Scientific, Waltham, Massachusetts, USA). Growth inhibition was calculated relative to the untreated (UT) control. Medium without bacterial inoculation was used as a blank.

2.2. Checkerboard assay for investigation of synergistic activity

The checkerboard method was applied as previously described to assess the combination index (CI) and fractional inhibitory concentration index (FICI) values [23]. For this assay, 96-well plates (Nest Scientific) were set up with varying concentrations of AZM and CHX along the x-axis and y-axis, respectively. Each well contained 10^3 CFU/mL of *Pseudomonas aeruginosa* (PAO1) and was incubated at 37 °C for 24 h with shaking. At the end of the incubation, turbidity was assessed both visually and by measuring optical density at 600 nm [24]. FICI value was calculated using Equation-1, where FICI $\leq$0.5 indicates synergism, 0.5 $<$ FICI $\leq$1.0 indicates additivity, and 1.0 $<$ FICI $\leq$4.0 indicates indifference [25,26]. As a secondary approach, the CI method, widely used in biological studies (including assessments of synergistic interactions between paired combinations of antimicrobials), was applied using Equation-2. In this method, CI $<$ 1 indicates a synergistic effect, CI $<$ 0.5 indicates a highly synergistic outcome, CI = 1 indicates an additive effect, and CI $>$ 1 indicates an antagonistic effect [23,27,28].

FICI = (MIC of D_1/MIC of D_1 plus D_2) + (MIC of D_2/MIC of D_1 plus D_2) (Equation-1)

$$CI = D_1/(Dx)_1 + D_2/(Dx)_2 \quad \text{(Equation-2)}$$

where $(Dx)_1$, representing the dose of the drug alone that inhibits the growth of cells by x% and $(Dx)_2$ is the dose of the drug D_2 alone that inhibits the growth of cells by x% (or the MIC for FICI determination).

2.3. Spot plating and MTT assays

The bacteria (10^3 CFU/mL in 250 μL TSB) were treated with the indicated concentrations of AZM and/or CHX in eppendorf tubes to ensure more homogeneous growth in suspension and ease of sample collection compared to 96-well plates. The bacteria were incubated at 37 °C with shaking (160 rpm) for 24 h under aerobic conditions, after which OD_{600} values were measured [29]. In experiments involving AZM, its solvent DMSO was included as a solvent control at the corresponding AZM concentrations, while untreated cells served as the untreated control (UT).

Growth inhibition was confirmed using the agar spotting method as previously described [19,29]. Briefly, following a 24 h incubation with varying concentrations of AZM, CHX, and CHX + AZM, the bacteria were serially diluted in TSB, and 3 μL of each dilution were plated onto TSA agar plates. After overnight incubation at 37 °C, bacterial growth on TSA plates was imaged using the Gel Logic-212 Pro imaging system (Carestream, USA). In cases where indicated, agar spot plate experiments were conducted using Cetrimide agar (selective for PA). Cetrimide agar was prepared by dissolving 45.3 g of *Pseudomonas* agar base and 10 mL of glycerol (Fluka, UK) in 1 L of dH_2O, followed by autoclaving for 15 min to sterilize. Following spot plating, the plates were incubated overnight at 37 °C and visualized under UV light using a transilluminator (DAIHAN Scientific, South Korea) [30].

Growth inhibition was also evaluated through metabolic activity measurements using the MTT (3-(4,5-dimethylthiazol-2-yl)-2,5-diphenyltetrazolium bromide) assay, as previously described with some modifications [31]. MTT stock solution was prepared by dissolving MTT

(BioVision, Pennsylvania, USA) in dH_2O at 5 mg/mL 15 μL of the bacterial culture was incubated with 100 μL of 0.25 mg/mL MTT reagent (diluted from the stock solution in phosphate-buffered saline, PBS) for 4 h with shaking at 37 °C. Subsequently, 100 μL of SDS solution (1 g SDS in 10 mL 0.01 M HCl in dH_2O) was added to each well, and the incubation continued overnight. Cell viability was monitored through the color change resulting from the dissolution of crystals formed by MTT reduction. Accordingly, viability was determined by measuring the absorbance at 570 nm using a microplate reader (Multiskan FC, Thermo Scientific). Absorbance values from wells containing MTT reagent inoculated with culture medium (15 μL) without bacteria were used as blanks.

2.4. Evaluation of biofilm

To determine the effect of AZM and CHX alone and in combination on biofilm formation, the PAO1 strain (10^3 CFU/mL) was incubated for 24 h in 96-well flat-bottomed polystyrene cell culture plates containing TSB medium at 37 °C under static conditions [32]. Untreated cells (UT) were used as controls. Following incubation, crystal violet (CV) staining was performed to determine the total biofilm biomass [33]. For this, after incubation, the medium from the wells was removed, and each well was washed three times with cell-culture grade PBS to remove planktonic bacteria. Then, 200 μL of methanol was added to each well, and the plates were incubated at room temperature for 15 min for fixation. After the removal of methanol, the wells were dried. Subsequently, 200 μL of 0.1 % (w/v, in dH_2O) CV was added to each well, and the plates were incubated at room temperature for 15 min. After removing the CV solution, the wells were washed at least three times with dH_2O, and after drying, 200 μL of 30 % acetic acid (v/v, in dH_2O) was added to each well to dissolve the CV. OD readings were determined at 550 nm using a microplate reader (Multiskan FC, Thermo Scientific). Absorbance values obtained from wells inoculated with medium without bacteria were used as blanks [32]. In parallel with CV staining, cell viability in the biofilm was also investigated using the MTT reduction assay as described above. Briefly, after removing the medium and washing the wells three times with PBS, 150 μL of the MTT solution (0.25 mg/mL) was added to each well. Following incubation at 37 °C with shaking for 4 h, 150 μL of SDS solution (1 g SDS in 10 mL 0.01 M HCl in dH_2O) was added to each well, and the incubation continued overnight. The absorbances were measured at 570 nm using a Multiskan FC (Thermo Scientific) microplate reader. Absorbance values from wells inoculated with medium without bacteria were used as blanks. The experiments were conducted as 5 biological replicates, each with at least 4 technical replicates. In this setup, the MTT to CV rate (MCR), a measure of the metabolic activity referring to the biofilm biomass, was calculated as described before [34]. For this, the normalized values of CV and MTT (CV_N and MTT_N, respectively) were determined according to Equation-3 and Equation-4 given below. MCR was calculated by taking the average of the MTT_N and CV_N (Equation-5). The MCR parameter is a measure of the metabolic activity referring to the biofilm biomass; however, high values for MCR can occur when the CV_N is relatively low. Therefore, a biofilm-specific activity (BSA) value is obtained by multiplying the MCR by the average of the MTT_N and CV_N (Equation-6), resulting in a descriptor of the MCR weighted by the average of the CV and MTT values [34].

$$CV_N = (CV - CV_{untreated\ control})/CV_{untreated\ control} \quad \text{(Equation-3)}$$

$$MTT_N = (XTT\text{-}MTT_{untreated\ control})/MTT_{untreated\ control} \quad \text{(Equation-4)}$$

$$MCR = MTT_N/CV_N \quad \text{(Equation-5)}$$

$$BSA = (MTT_N/CV_N) \times [(CV_N + MTT_N)/2] \quad \text{(Equation-6)}$$

To support the findings of the MTT assay, the biofilms were dispersed after washing three times with PBS following the removal of the medium containing planktonic cells, in order to determine if the treatments affected the number of viable cells in the biofilm. After the washing steps, 200 μL of 0.1 % (v/v, in PBS) Tween-20 was added to each well of the 96-well plate, and the plate was incubated at room temperature for 15 min on a horizontal shaker. At the end of the incubation period, 200 μL of cells from each well were collected, diluted in 2 mL of PBS, and used for agar spot plating at the indicated dilutions.

In addition to determining the viability of the cells in the biofilm structure, the viability and metabolic activity of the planktonic cells during the static culture for biofilm formation were also investigated. For this, at the end of the 24 h incubation, the bacterial suspension in the wells was collected, and planktonic cell density was determined through OD_{600} readings. The metabolic activity of the planktonic cells was assessed using the MTT assay with 15 μL of the cell suspension, as described above. Finally, the pyocyanin content of the suspension was also measured at 350 nm [35].

2.5. In vitro wound infection model

The combined effect of CHX and AZM on a collagen gel matrix wound model was investigated using previously described methods with some modifications [36,37]. Based on the inhibition results in broth culture, the CHX and AZM concentrations with the highest inhibition were selected: collagen wound model experiments were conducted using 1.5 μg/mL CHX and 2 and 4 μg/mL AZM. To prepare the matrix, 1 mL of 0.1 % acetic acid was added to 2 mL of the collagen stock solution (High Concentration Rat Tail Collagen Type I Collagen Solution, 10 mg/mL, Cat no: IKD119261001, Advanced Biomatrix, UK), and kept on ice. Simulated Wound Fluid (SWF) was prepared with 50 % v/v Fetal Bovine Serum (FBS; Biological Industries, Israel) and 50 % v/v Peptone Water (0.1 % w/v Peptone in 0.9 % w/v NaCl) and cooled on ice. Then, 6 mL of SWF was added to the collagen solution on ice. The pH was adjusted to 7.5 with 1 mL of 0.1 M NaOH. The mixture was pipetted into 96-well cell culture plates (100 μL per well) on ice, avoiding bubble formation. The collagen matrix was incubated at 37 °C for 1 h to solidify. PAO1 grown overnight in liquid culture was diluted in SWF to 10^3 CFU/mL, and AZM, CHX, or the AZM and CHX combination was added to the bacterial suspension. 50 μL of the bacterial suspension was added to the collagen-containing wells and incubated statically at 37 °C for 24 h. Collagen incubated with SWF alone served as the negative control. At the end of the incubation, a significant change in pyocyanin production with treatment was observed and photographed.

To investigate the effectiveness of treatment post-infection, the collagen matrix was first inoculated with PAO1 (as described above). After 24 h, AZM and CHX were applied individually and in combination, followed by an additional 24 h incubation. At the end of this period, the MTT assay was performed, and fluorescence microscopy images were taken, as described below.

For quantitative analysis of viable (metabolically active) bacteria adhered to the collagen at the end of the incubation period, the MTT assay was performed. Additionally, bacteria collected from the collagen were plated on TSA agar for colony counting. For these experiments, collagenase (Collagenase from Clostridium histolyticum, Cat no: C0130-100 MG, Sigma-Aldrich, Germany) was prepared at 4 mg/mL in 20 mL PBS (PBS with Ca^{2+} and Mg^{2+} for collagenase activity) containing 5 mL FBS, aliquoted, and stored at −20 °C. The working concentration was 500 μg/mL in PBS with Ca^{2+} and Mg^{2+} (cell culture grade). For the MTT assay, the liquid on the collagen surface was removed, and 100 μL of collagenase was added to each well, followed by incubation at 37 °C for 1.5 h. The well contents were pipetted, and 20 μL was transferred to new 96-well plates. 100 μL of MTT reagent (0.25 mg/mL) was added to each well, and the plates were incubated at 37 °C for 4 h in a shaking incubator. Then, 100 μL of SDS-HCl solution (described above) was added to each well, and after overnight incubation, the color change was measured at 570 nm.

2.6. Propidium iodide staining

After 24 h of incubation, the SWF on the collagen surface was removed, and methanol, stored at −20 °C, was carefully added to each well while keeping the plate on ice. The plate was incubated at −20 °C for 10 min. Then, methanol was removed, and 200 μL of propidium iodide (PI; 1 μg/mL in PBS) was added to each well. After overnight incubation at 4 °C in the dark, the PI solution was removed. A pipette tip was cut to fit into each well, and collagen was carefully transferred to slides for microscopic observation using an Olympus BX53 fluorescence microscope with a U-FGNA filter (excitation: 535 nm, emission: 617 nm) at 20X and 40X magnification. Exposure was 13.02 ms, the same for all groups.

2.7. Culturing and treatment of mammalian epithelial cells with chlorhexidine and azithromycin

HT-29 (ŞAP Enstitüsü, Ankara, Türkiye) and HCT-116 (DSMZ, Braunschweig, Germany) CRC lines were cultured in RPMI-1640 without phenol red (Capricorn Scientific, Germany) containing 10 % FBS (Biological Industries), 2 mM L-glutamine and 1 % penicillin/streptomycin as previously described [20,38]. The day before the treatment, the cells were seeded as $1x10^4$ cells/well of a 96-well plate. The cells were treated with CHX, AZM or both for 24 h at 37 °C in a humidified atmosphere of 5 % CO_2 and 95 % air. Since AZM is dissolved in DMSO, cells treated with an equal volume of DMSO served as controls. Untreated cells (UT) were also used as controls. At the of the incubation period, the medium was removed and the MTT assay was performed as previously described [30]. Briefly, the cells were incubated for 4 h at 37 °C in 100 μL of complete RPMI-1640 medium containing 1.2 mM of MTT reagent (BioVision). Following the incubation, 100 μL of an SDS solution (1 g of SDS in 10 mL of 0.01 M HCl) was added to dissolve the MTT formazan crystals. Subsequently, the plates were further incubated at 37 °C for 16 h. The absorbances were measured at 570 nm using a microplate reader (Thermo Fisher Scientific). Absorbance values which were read from the wells without cells but containing complete medium with MTT and SDS solutions were used as blanks. Before the MTT assays, cells were observed under an inverted light microscope (Nikon Eclipse TS100, Japan) and images were captured using a Toupcam HD camera China (China).

2.8. Fourier Transform Infrared Spectroscopy (FTIR) analyses

To determine whether the combined use of AZM and CHX affects each other's cellular accumulation compared to when used alone, Attenuated Total Reflection- Fourier Transform Infrared Spectroscopy (ATR-FTIR) was employed. Bacteria treated with AZM and/or CHX for 24 h, or untreated (UT), had their OD_{600} values measured. The bacteria, at a concentration of 10^8 CFU/mL, were then washed twice with cell culture-grade PBS at room temperature using a bench-top centrifuge set to 5000 rpm (1844×*g*) for 10 min [39]. A 2 μL aliquot of the bacterial suspension in cell culture grade PBS at 10^8 CFU/mL was placed on the crystal of the ATR unit, dried with inert nitrogen gas (N_2) for 5 min, and analyzed using an ATR-FTIR spectrometer (PerkinElmer, Spectrum 100, Waltham, Massachusetts, USA) at a resolution of 2 cm^{-1}, with 32 scans over a spectral range of 4000-650 cm^{-1}. Four spectra were obtained for each bacterial sample. The spectra of the PBS and agents in PBS at concentrations of 1.5 μg/mL CHX and 2 μg/mL AZM were also recorded.

Before analysis, the data were processed using Spectragryph v1.2.16.1 software, applying ATR-baseline correction, 3rd-degree polynomial Savitzky-Golay smoothing, and vector normalization [40]. Peaks in PBS samples containing AZM or CHX were identified using the integrated peak determination feature of Spectragryph v1.2.16.1, with the most sensitive detection settings applied (threshold 0.01 %, scan range 4, and peak position tolerance 0.01 %). The detected peaks were then compared within a ±1 cm^{-1} margin to distinguish those unique to PBS, AZM, or CHX (e.g., CHX-specific peaks distinct from AZM, and vice versa). Biologically active concentrations of both agents were used for peak identification in this study. Once the distinctive peaks for AZM and CHX in PBS were identified, ATR-FTIR spectra of bacteria treated with AZM and/or CHX or left untreated were analyzed to locate the AZM and CHX peaks previously determined in PBS. Peaks identified in cells treated with both AZM and CHX (but absent in untreated controls) and peaks exclusive to AZM-treated samples (absent in CHX-treated samples) were designated as AZM-specific. Similarly, peaks observed in both AZM and CHX-treated cells (but absent in untreated controls) and peaks unique to CHX-treated samples (absent in AZM-treated samples) were considered CHX-specific. Relative quantification of cellular AZM and CHX accumulation was performed by analyzing baseline-corrected peak areas, selected based on the positions of the identified cellular AZM- and CHX-specific peaks.

2.9. Statistical analysis

The experiments were repeated as at least two biological replicates with at least two technical replicates and presented as mean ± SEM. Statistical significance was determined using the *t*-test and the degrees of significance are indicated with asterisks (*), as follows: *p ≤ 0.05, **p ≤ 0.01, ***p ≤ 0.001, ****p ≤ 0.0001. Statistical significance was determined compared to the untreated control group (UT), with intergroup comparisons made where indicated. GraphPad Prism 8 (La Jolla, CA, USA) and OriginPro 2021 v 9.8.0.200 software were used for data analysis and graphing.

3. Results

3.1. The combination of chlorhexidine and azithromycin demonstrated enhanced growth inhibition

In PAO1, the MIC for AZM was determined to be 70 μg/mL, while for CHX, it was 6 μg/mL. For FICI and CI calculations, MIC values were combined with the checkerboard assay results to evaluate the nature of the interaction between CHX and AZM (Supplementary Fig. 1), yielding an index of 0.61. Notably, this value suggests a synergistic effect, as a CI < 1 indicates synergy [23]; however, it exceeds the FIC index threshold for synergy (0.5) but falls within the range for additivity (FICI ≤1.0).

The subsequent biological evaluations of the combination were performed using 2 and 4 μg/mL AZM and 1 and 1.5 μg/mL CHX. The growth inhibition results obtained after 24 h treatments with CHX and AZM alone and in combination at these concentrations are shown in Fig. 1A as relative to the untreated (UT) control (on the left) which was confirmed by agar spot plating (on the right). The difference in culture densities after 24 h was photographed to show the dramatic effect of the combined treatment and growth inhibition (lower panel). Notably, considering the stock concentration, the DMSO ratio for 2 and 4 μg/mL AZM is 0.02 ‰ and 0.04 ‰ by volume, respectively. At these ratios, DMSO (the solvent) did not affect bacterial viability (Supplementary Fig. 2). Serving as an indicator of cell cytotoxicity, viability, and proliferation [20], cell viability was also confirmed using the MTT reduction assay (Fig. 1B).

In a previous study on *Acinetobacter baumannii*, an opportunistic nosocomial pathogen, it was shown that the combination of CHX with minocycline, doxycycline, meropenem, or ciprofloxacin exhibited synergistic responses across all clinical isolates, with over 50 % showing FICI ≤0.5. Notably, combinations with imipenem or levofloxacin displayed indifferent effects in 10 % and 3.33 % of isolates, respectively. Overall, CHX combined with these six antibiotics demonstrated synergistic or additive effects [7]. Here, based on OD_{600} data, 1.5 μg/mL CHX caused an 11.4 ± 4 % inhibition, 2 μg/mL AZM resulted in a 14 ± 4.5 % inhibition, and 4 μg/mL AZM led to a 30.5 ± 4.7 % inhibition in PAO1. However, the combination of 1.5 μg/mL CHX and 2 μg/mL AZM achieved a 58 ± 6 % inhibition, significantly exceeding the sum of their

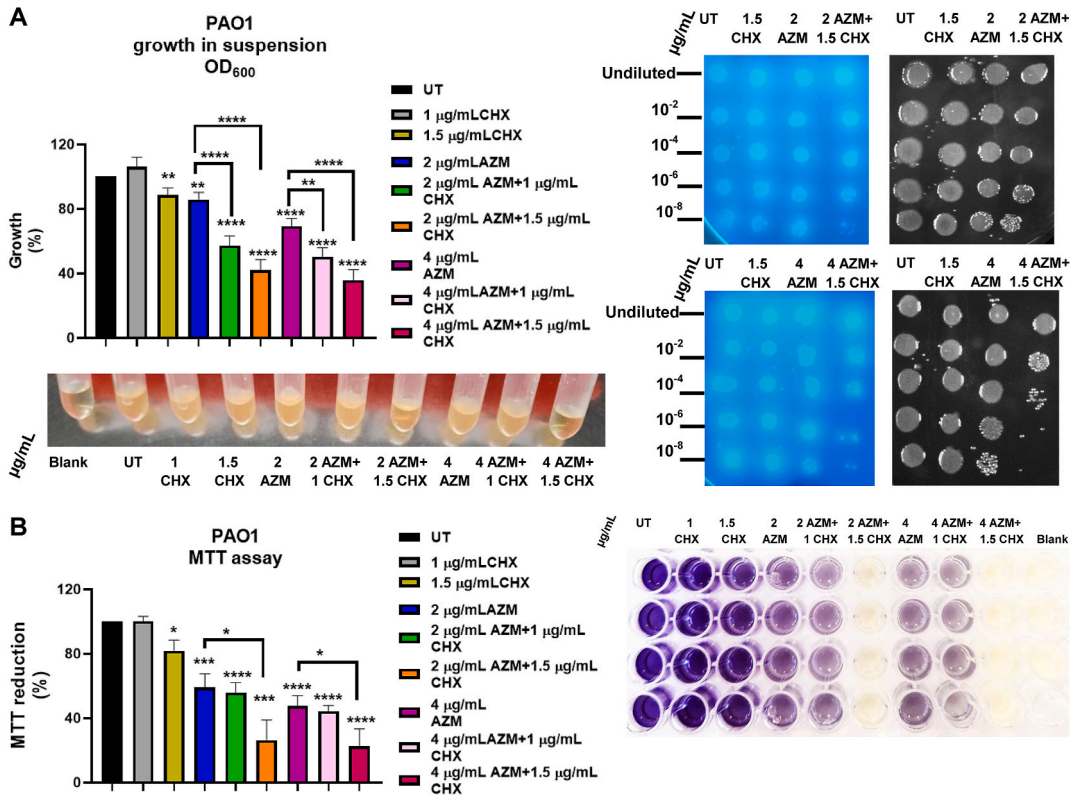

Fig. 1. Effect of CHX and AZM combination on the growth inhibition in *P. aeruginosa* (PAO1). A. The growth inhibition results based on OD_{600} measurements with CHX and AZM alone and in combination are shown (on the left), which was confirmed by agar spot plating (on the right). The difference in culture densities after 24 h was photographed and presented in the lower panel. B. MTT assay results 24 h post-treatment with CHX and/or AZM (on the left) and a representative plate image (on the right) are shown. The results are given as mean ± SEM and presented relative to UT control. *t*-test was applied to compare with UT and for comparisons between the treatment groups as indicated.

individual effects. Similarly, the combination of 1.5 μg/mL CHX and 4 μg/mL AZM produced a 64 ± 6 % inhibition, clearly demonstrating that the combined effect surpasses an additive outcome. These results indicate that the combination of AZM and CHX exerts a markedly greater inhibitory effect compared to either agent alone, with the most pronounced inhibition observed for the combination involving 1.5 μg/mL CHX in this experimental setup.

3.2. The combined treatment changed the biofilm nature

Biofilm biomass after treatment with CHX and AZM alone and in combination was determined using CV staining. The CV colorimetric measurement results are shown in Fig. 2A as percentages relative to the untreated control group (left panel), with a representative plate image presented in the right panel. The results indicate that with the combined treatment, the density of the CV staining increased. CV binds nonspecifically to both matrix components and live and dead bacterial cells, making it unsuitable for assessing the activity of biofilm cells [41]. Therefore, while CV staining indicates biomass, it does not reflect cellular activity [33]. To measure cellular metabolic activity as an indicator of cell viability, proliferation, and cytotoxicity, the MTT assay was employed [20,33,42] as the results are shown in Fig. 2B with a representative plate image on the right. These results indicate that although the biofilm biomass increased with the combination of AZM and CHX, as suggested by CV staining data, the cells within the biofilm were not alive (or metabolically active). This decrease in cellular viability within the biofilm structure, associated with the combined treatment, was further confirmed through the agar spot plating assay. Additionally, the decreased MTT to CV ratio (MCR; on the left) and biofilm-specific activity (BSA; on the right) corroborate the effect of the combined treatment on the biofilm's nature (Fig. 2C).

Only live bacteria within the biofilm can transition to a planktonic form, potentially initiating a new infection or forming a biofilm at another location [43]. This phenomenon can be explained by the dispersion process [44]. Thus, after demonstrating the decreased number of viable cells in the biofilm, the viability of the cells in the suspension was also assessed. Supplementary Fig. 3 shows the effect of AZM treatment on the viable cell count in the suspension, which was further decreased with the AZM and CHX combination. Therefore, the reduced bacterial density in suspension with the combination treatment indicates the inhibitory effect of the combined treatment on planktonic cells and may also reflect a reduction in dispersion capability, a marker of virulence [45].

In PA, pyocyanin, a pigment that can be tracked in culture media due to its greenish color [46] and a positive correlation has been found between antibiotic resistance and pyocyanin production in PA strains isolated from patients with hospital-acquired wound infections [47]. Increased pyocyanin production and release in PA has been reported as a virulence factor by improving bacterial adhesion and biofilm formation [46–48]. In this study, the change in pyocyanin production in the PAO1 culture incubated statically for 24 h was monitored through color change, and the changes in absorbance values were measured at 350 nm. Supplementary Fig. 4 shows the changes in pyocyanin production relative to the untreated control group. Accordingly, the production of pyocyanin significantly decreased mainly with AZM treatment; on the other hand, the combination with CHX slightly enhanced the effect of AZM.

Collectively, it can be concluded that biomass stained with CV is partially related to biofilm pathogenicity, as indicated by the decrease in the count of viable cells and cell metabolism associated with biofilm, and pyocyanin synthesis.

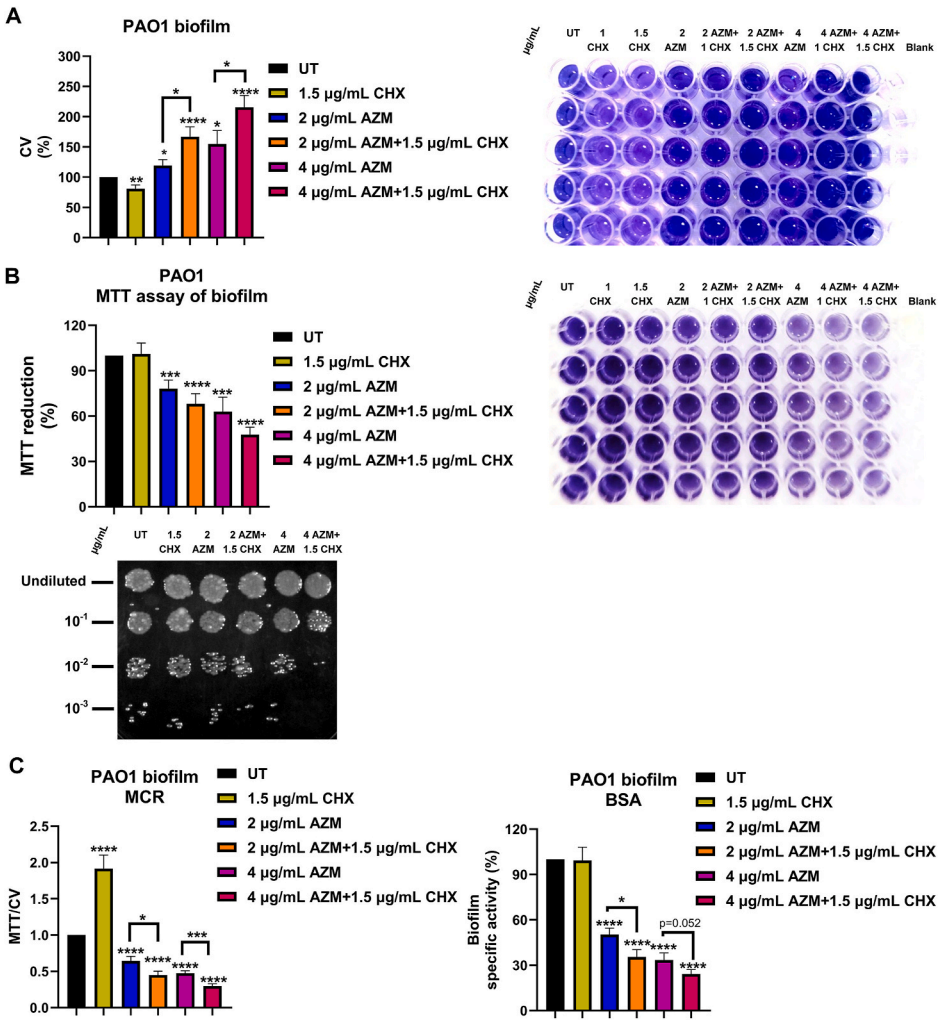

Fig. 2. CHX and AZM combined treatment changes biofilm mass and viability in *P. aeruginosa* (PAO1) biofilm. **A.** The crystal violet (CV) staining results for biofilm mass determination in the 24 h static cultures of PAO1 are shown (left panel), with a representative plate image on the right. B. The results of the MTT assay applied to the biofilm are shown in the left panel, and a representative plate image is presented on the right. The changes in bacterial viability in the biofilm were also shown by agar spot plating (lower panel). C. For the 24 h biofilm, the MTT to CV ratio (MCR) is shown on the left, and biofilm-specific activity (BSA) is given on the right. The results (mean ± SEM) are presented as percentages relative to the untreated (UT) control. *t*-test was used for comparisons with the untreated control group and intergroup comparisons.

3.3. The combination of chlorhexidine and azithromycin enhanced the inhibitory effect in the in vitro wound infection model

The efficacy of AZM (2 and 4 µg/mL) and CHX (1.5 µg/mL) combination was investigated through experiments examining PAO1 growth in a serum-supplemented collagen matrix. Similar to the results obtained for suspension cultures (Fig. 1), the agents demonstrated an enhanced effect in inhibiting bacterial growth, as evidenced by the MTT assays shown in Fig. 3A (left panel), with a representative plate image on the right. The reduction in pyocyanin production after 24 h of incubation is also visible (top right). The results were further validated by colony counting experiments, which aimed to detect viable bacteria (Fig. 3B). The decrease in bacterial density treated with AZM and CHX was also confirmed by PI staining shown in Fig. 3C.

To assess the effectiveness of the treatment in a post-infection model, the matrix was treated with CHX and AZM alone or in combination for an additional 24 h, following a 24 h initial incubation with PAO1 without CHX or AZM. The results suggest an enhanced effect of the combined treatment (Supplementary Fig. 5).

Collagen and serum proteins promote bacterial adherence to surfaces, a process that negatively impacts wound healing, particularly in chronic wounds [36,37]. The results indicate that CHX and AZM combination exhibit an enhanced inhibitory effect on PAO1 infection in the *in vitro* wound matrix structure.

3.4. Chlorhexidine supports the cellular accumulation of azithromycin

To investigate whether the enhanced inhibitory effect of the combination results from increased bacterial accumulation of one or both agents, a spectral method was employed for the first time in the literature. For this, the ATR-FTIR spectra for CHX (1.5 µg/mL) and AZM (2 µg/mL) in cell-culture grade PBS were obtained (Supplementary Fig. 6A). Characteristic absorption bands are reported at around 3325-3323 cm^{-1}, 3119 cm^{-1}, 2956.7 cm^{-1}, and 2542 cm^{-1} for N-H stretching, 1519.8 cm^{-1} for N-H bending, 1610 cm^{-1} and 1489 cm^{-1} for C = C aromatic bending, 1650, 1600, 1550, and 1500 cm^{-1} for C = C aromatic stretching, 1259.4 cm^{-1} for C–N aromatic stretching, 1022.2, 1093, and 1155.3 cm^{-1} for C-N stretching, and 2947 cm^{-1} for C-H stretching are reported in the literature for the IR spectrum of CHX [49–53]. The FTIR spectrum presented in Supplementary Fig. 6A is consistent with the FTIR spectrum of CHX in the database (https://spectrabase.com/spectrum/AbZKEOrkYAi). For AZM, the descriptive FTIR absorption bands in the literature are defined as follows: C-H at 3020-2750 cm^{-1} and 1377 cm^{-1}, -OH at 3648 and 3560 cm^{-1}, -CH3 at 2973 and 2830

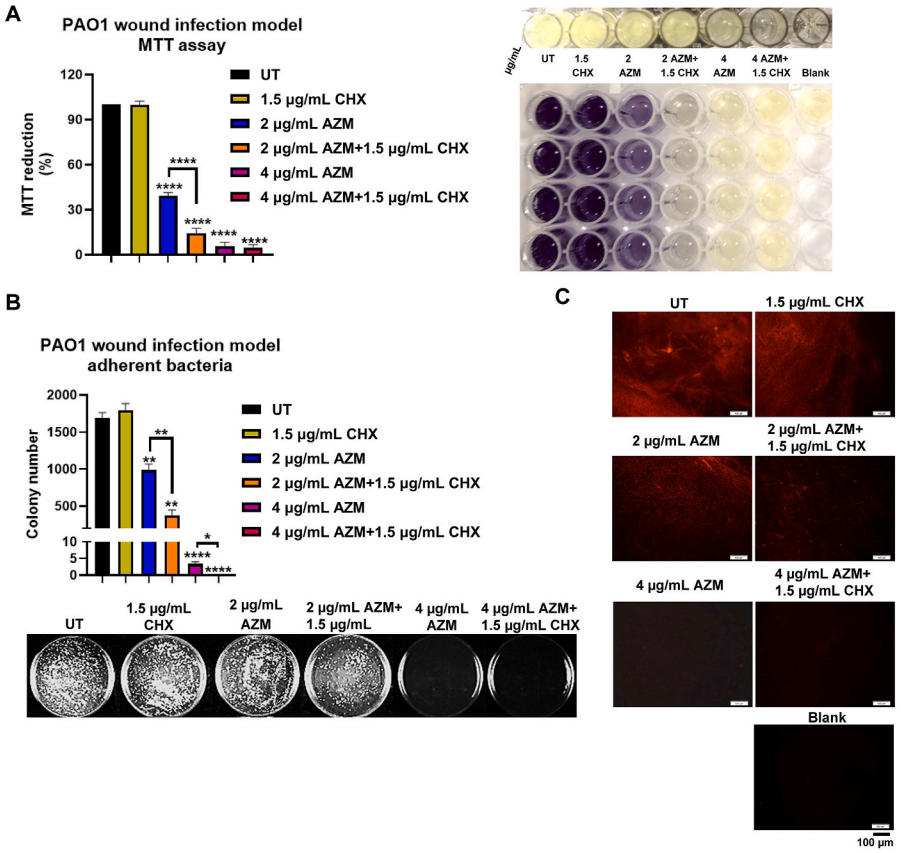

Fig. 3. CHX and AZM co-treatment is effective in a wound infection model with *P. aeruginosa* (PAO1). A. CHX and AZM co-treatment resulted in enhanced activity in inhibiting PAO1 growth, shown by the MTT assay applied to the serum-supported collagen matrix incubated with the pathogen for 24 h (left panel; presented as % relative to the untreated control-UT). In the top of the right panel, the reduction in pyocyanin production is presented. Below it, a representative plate image from the MTT assay is given. B. At the end of the 24 h incubation, the viable bacteria associated with the collagen matrix were evaluated through spread plating. The colony counting results are shown at the top, and the representative plates are shown at the bottom. C. The density of the pathogen associated with the matrix at the end of the 24 h incubation was evaluated by propidium iodide (PI) staining. The results are given as mean ± SEM and *t*-test was used to compare with the UT and for comparisons between the treatment groups as indicated.

cm^{-1}, and O=C=O stretching at 2323 cm^{-1}; the region of 1744-1709 cm^{-1} especially for axial C=O stretching at 1724 and 1719 cm^{-1}, C-O axial stretching at 1221-1134 cm^{-1}, stretching for R-O-R types at 1189 cm^{-1}, and a minor band for C-N stretching at 1090 cm^{-1} [54–56]. The ATR-FTIR spectrum of AZM in PBS is also in accordance with the literature and accessible FTIR spectrum in the database (https://spectrabase.com/spectrum/E4cRH6RERPb). In this study, specific bands presented in Table 1 have been identified for the concentrations of AZM and CHX utilized in ATR-FTIR analyses. The peaks delineated in the table were derived from the spectra depicted in Supplementary Fig. 6A using the integrated peak determination feature of Spectragryph v1.2.16.1 software. Subsequently, the obtained peaks were compared with a ±1 cm^{-1} margin to discern peaks distinct from those of PBS and from each other (i.e., for CHX, distinct from AZM, and for AZM, distinct from CHX).

Following the identification of the specified peaks regarding AZM and CHX in PBS, ATR-FTIR spectra of bacteria treated with AZM and/or CHX or left untreated were examined. The average ATR-FTIR spectra of four replicates are presented in Supplementary Fig. 6B. In Table 1, the peaks identified for AZM and CHX in PBS that were also detected in bacterial samples are highlighted in bold. The ATR-FTIR spectra of bacteria untreated and treated with CHX and/or AZM were subjected to multivariate analysis. The loading plots belonging to the Principal Component Analysis (PCA) are shown in Fig. 4A and B. The scores for principal components 1 and 2 (PC1 and PC2) were 87.2 % on the PC1 plane and 8.2 % on the PC2 plane, indicating that the bacterial groups were distinguished with a score of 95.4 % (Fig. 4C). It is observed that although the CHX-treated samples differed from the untreated (UT) samples on the PC1 plane, CHX was closer to the UT samples compared to AZM and the AZM and CHX co-treated samples. On the PC2 plane, it can be said that the UT and AZM-treated samples did not differentiate, but the CHX and AZM and CHX co-treated samples did. The CHX group showed the most significant differentiation from the UT on the PC2 plane. In summary, it can be suggested that a substantial proportion of the variance (PC1) can be explained by the effects of AZM treatment, and the second principal component (PC2) seems to correspond to the CHX treatment-dependent changes.

In the combined application of CHX and AZM, to determine whether one agent affects the cellular accumulation of the other, the peaks identified as belonging to AZM or CHX in Table 1 and highlighted in bold were used. From these peaks, those detected in the ATR-FTIR spectra of cells treated with both AZM and CHX (but not found in the untreated control group, UT) and those found in samples treated only with AZM (and not in samples treated only with CHX) were described as AZM-related peaks. Similarly, those detected in the ATR-FTIR spectra of cells treated with both AZM and CHX (but not found in the untreated control group, UT) and those found in samples treated only with CHX (and not in samples treated only with AZM) were described as CHX-related peaks. The most prominent AZM and CHX-related peaks are presented in Supplementary Fig. 7. In AZM-related bands, the peaks around 2749 [57], 2650 cm^{-1} [58,59] and 2645 cm^{-1} [60,61] are assigned to C-H stretching, 1746 for the C=O group [62–64] and 1345 cm^{-1} assigned to N-O stretching [65], and 1334 for C-N moiety [66]. For CHX, the identified peaks were around 2510 cm^{-1} [67] and 2366 cm^{-1} assigned for NH [68], 2247 cm^{-1} [69], 1390 [70], 1196 [71],1185 [71]

Table 1
Spectral peaks detected for AZM and CHX in PBS[a]

AZM		CHX	
Wavenumber (cm^{-1})	Absorbance	Wavenumber (cm^{-1})	Absorbance
2924.4	0.021983	2991.7	0.010003
2762.3	0.012977	2957.6	0.016416
2749.3	**0.012369**	2954.4	0.016176
2650.6	**0.0088785**	2685.3	0.010262
2645.2	**0.006673**	2659.7	0.010194
2630.6	0.006269	2619	0.0057165
2605.5	0.0032746	2598.7	0.0047517
2585.4	0.001505	**2510.7**	**0.003891**
2487.1	0.004198	2503.3	0.0041509
2467.3	0.0048896	2426.9	0.0071725
2360.4	0.033302	**2365.7**	**0.031391**
2321.1	0.037741	2281	0.022107
2258.7	0.017828	2273.6	0.022828
2168.9	0.0083819	**2247.6**	**0.016941**
2109	0.01401	2240.7	0.016177
1921.8	0.010465	2220.3	0.012171
1914.2	0.010295	2209.4	0.012367
1861.9	0.0097159	2064.9	0.014576
1801.8	0.0072227	2044.6	0.0076507
1746.2	**0.0042993**	1904	0.014394
1642	0.028642	1599.5	0.013757
1567.2	0.011341	1479.2	0.003464
1500.9	0.0062142	1450.7	0.0057267
1345.1	**0.003821**	**1444.8**	**0.004749**
1334.1	**0.004301**	1432.1	0.005386
1283.9	0.0055696	1403.5	0.0058426
1277.1	0.0057389	**1394.2**	**0.005429**
1241.6	0.0029073	1383	0.0050252
1004.9	0.00879	1333.4	0.0027492
927.84	0.007383	**1302.5**	**0.003**
876.17	0.013622	**1282.5**	**0.003852**
775.75	0.004895	1269.7	0.0045942
749.82	0.0034056	1261.6	0.0041608
		1251.6	0.0030553
		1224	**0.0014085**
		1196.7	**0.00080028**
		1191.5	0.0014428
		1185.9	**0.0017226**
		1176.7	**0.0036544**
		1164.1	0.0053136
		1134.8	0.013639
		1086.3	0.041786
		984.28	0.012076
		951.58	0.0057625
		867.93	0.010217
		835.83	0.007526
		825.01	0.0057823
		820.59	0.0053354
		816.41	0.0052009
		801.59	0.0038431
		785.15	0.0026311

[a] The peaks highlighted in bold were also detected in treated bacterial samples but not in untreated samples.

and 1176 cm^{-1} for CN [72], 1301 and 1283 (1301-1229 cm^{-1}) for C-N stretching, N-H bending [73], 1441 and 1224 for C(ring)-N and C-C groups [74]. As a side note, it has been observed that some of the peaks provided for CHX in PBS exhibit slight shifts in the ATR-FTIR spectrum of cells treated with CHX: the peak obtained at approximately 1444 cm^{-1} in the ATR-FTIR spectrum of PBS is observed at 1441 cm^{-1} in bacterial samples, the peak obtained at 1394 cm^{-1} in PBS is observed at 1390 cm^{-1}, and the peak obtained at 1302 cm^{-1} in PBS is observed at 1301 cm^{-1}. However, no significant shift is observed among the peaks of interest in cells treated with AZM compared to the ATR-FTIR spectrum of AZM in PBS.

For relative quantification, baseline-corrected peak areas which were selected based on covering the positions of the cellular AZM and CHX-related peaks were used. The start and end points of the baseline for bacteria samples treated with CHX were 2512.90–2509.60 cm^{-1}, 2367.10–2364.14 cm^{-1}, 2248.88–2242.23 cm^{-1}, 2223.17–2218.62 cm^{-1}, 1442.47–1439.83 cm^{-1}, 1396.50–1393.18 cm^{-1}, 1285.77–1282.89 cm^{-1}, 1225.48–1221.26 cm^{-1}, 1198.92–1194.48 cm^{-1}, 1180.35–1175.70 cm^{-1}, and 1189.52–1183.87 cm^{-1} and for AZM were 2751.68–2744.73 cm^{-1}, 2646.72–2636.82 cm^{-1}, 2654.08–2646.56 cm^{-1}, 1747.70–1743.04 cm^{-1}, 1350.95–1342.14 cm^{-1}, and 1337.59–1333.04 cm^{-1}. The peak areas corresponding to these regions for combined treatment and CHX- or AZM-only samples are provided in Supplementary Table 1 and Supplementary Table 2. Fig. 4D shows the relevant peak areas as fold changes for the combined applications compared to the applications with each agent alone. As can be seen, the peak areas related to CHX do not change with the combined AZM and CHX treatment (left panel). However, there is a prominent and significant increase (more than 2-fold) in the samples co-treated with AZM and CHX compared to the AZM-only group (right panel). This result suggests that CHX treatment can increase the bacterial accumulation of AZM.

To determine if the treatments specifically affect lipids and proteins, changes induced by CHX and/or AZM were analyzed using FTIR spectra. Fig. 4E shows the ratio of the integrated peak area (1737-1730 cm^{-1}) for ester bonds, attributed to the C=O stretches of ester functional groups [75–77] to the sum of the integrated intensities of CH_2 symmetric and asymmetric stretching bands (2859-2842 cm^{-1} [78,79] and 2928-2916 cm^{-1} [79,80]) which correspond to saturated lipids and indicate the total lipid content [79]. It appears that when the agents are applied together, the amount of ester bond formation (between fatty acids and glycerol) decreases significantly compared to when the agents are used alone. This result can support the enhanced cellular accumulation of AZM through potential alterations in membrane lipid content and organization.

Since AZM functions as a protein synthesis inhibitor, changes in the protein content of the cells when the agents are applied alone or in combination were analyzed. For this, the integrated peak areas for Amide I (C=O stretching; 1696-1671 cm^{-1}) and Amide II (NH bending; 1550-1516 cm^{-1}) [81] were calculated. As shown in Fig. 4F, AZM treatment causes a significant decrease in cellular protein content, while co-treatment with AZM and CHX increases the protein content. The Amide I band is widely used to study protein structural changes [82]. The observed pattern in the changes in Amide I and Amide II areas suggests that the presence of CHX modulates the expression of genes affected by AZM. This can be supported by the finding that AZM-dependent translational inhibition is selective; in other words, AZM acts as a context-specific ribosome modulator (rather than a universal inhibitor), where the fate of the protein synthesized by the macrolide-bound ribosome is defined by its amino acid sequence [83]. It is possible that during co-treatment, the translated protein repertoire of the cell changes. This may explain the similar changes in the Amide I band, related to protein backbone conformation and a source of important structural information [82], and the Amide II band.

3.5. The combination offers an enhanced anti-growth effect on *Streptococcus mutans*

To determine whether the enhanced anti-growth effect of the combined AZM and CHX treatment, compared to each agent alone, is specific to Gram-negative bacteria like *P. aeruginosa* and *E. coli* [19], growth inhibition experiments were conducted with *S. mutans*, a Gram-positive pathogen primarily found in the human oral cavity and an important etiologic agent of dental caries [20]. The OD_{600} measurements demonstrated that, when used together, AZM (2 and 4 μg/mL) and CHX (0.5 μg/mL) achieve a greater inhibitory effect on *S. mutans* growth compared to their individual effects and exceed the sum of their inhibitory activities when used alone (Fig. 5). This inhibition was further confirmed by the agar spot assay, as shown in the right panel of Fig. 5.

CHX is used as an oral disinfectant [84]. A 0.2 % CHX solution has been shown to effectively reduce salivary *S. mutans* counts [85]. *In vitro*,

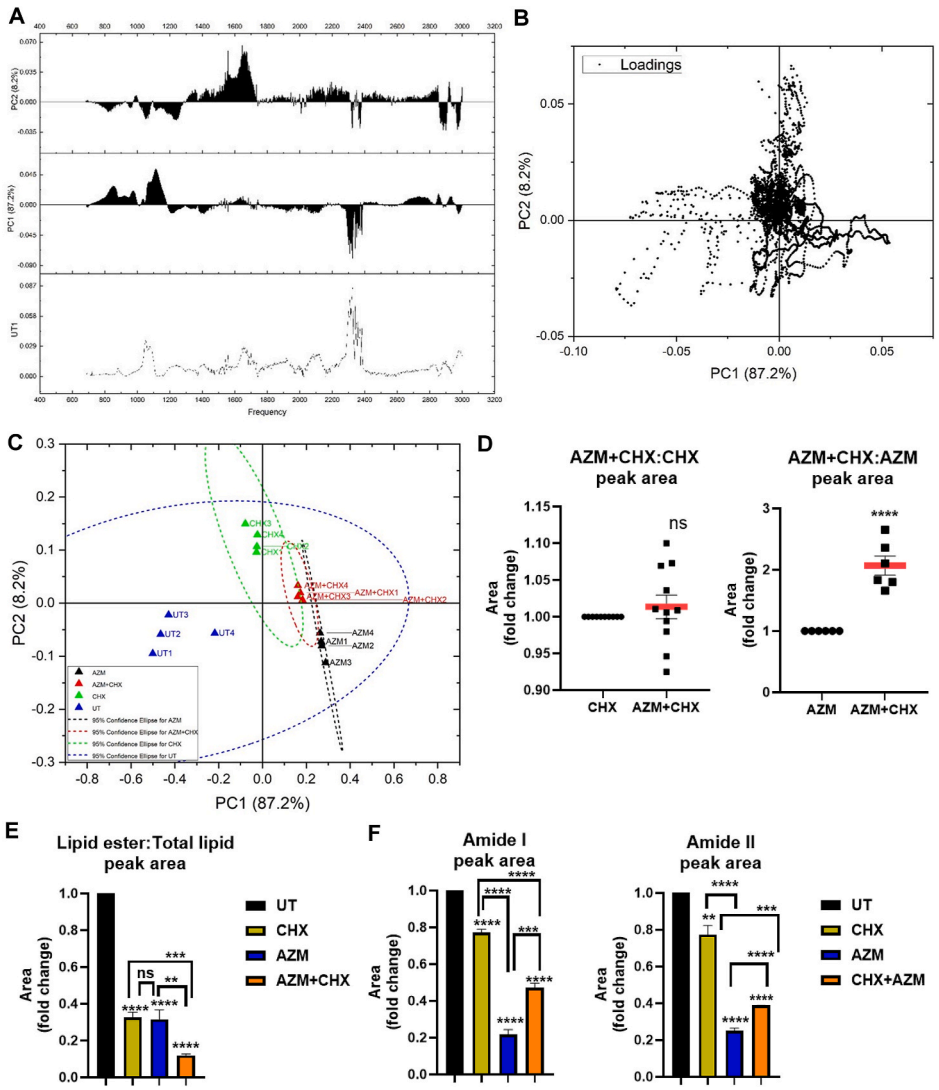

Fig. 4. FTIR analysis reveals distinctive features of the co-treatment. A. The loading plot with the reference spectrum (untreated; UT), B. The loading plot with the principal components PC1 and PC2 and C. The score plot of the principal component analysis (PCA) are shown. D. The integrated peak areas for the cell-associated CHX and AZM are presented as fold changes respect to the areas belonging to the combined treatment. Each spot represents an individual spectral band peak range area. E. The ratio of the peak area for C=O stretches of ester functional groups to the sum of peak areas for CH_2 symmetric and asymmetric stretching bands is shown as a normalized ratio relative to the UT. F. Peak areas for the Amide I and Amide II regions are presented as fold changes relative to the untreated control (UT). Spectral data were obtained from bacteria treated with 1.5 μg/mL CHX and/or 2 μg/mL AZM and grown in suspension for 24 h aerobically. Results are presented as mean ± SEM. *t*-test was used for comparisons with UT and between treatment groups.

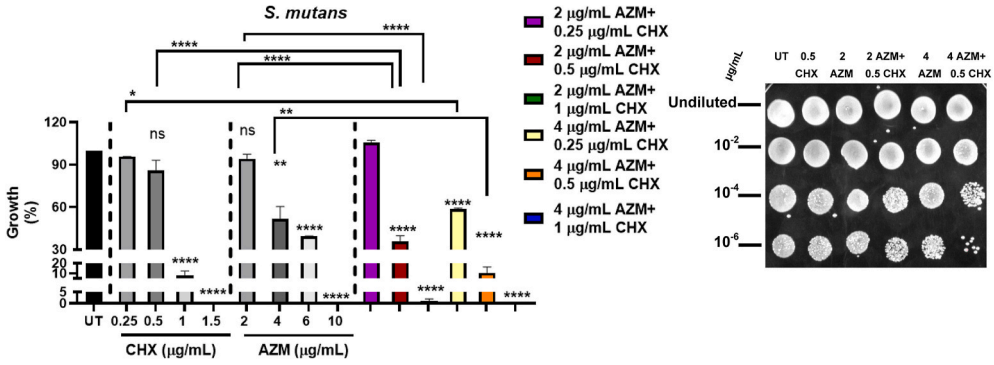

Fig. 5. CHX and AZM combined treatment shows enhanced growth inhibitory activity on the oral pathogen *S. mutans*. A. After 24 h of incubation in suspension culture, the growth of *S. mutans* treated with the agents alone or in combination was analyzed through OD_{600} measurements. The results are presented as % inhibition relative to the untreated control (UT) and shown as mean ± SEM. Growth inhibition was further assessed through agar spot plating assay. *t*-test was used for comparisons with UT and between the indicated treatment groups.

a concentration of 1.25 μg/mL CHX has been reported as the MIC value for *S. mutans* [84], which is consistent with the findings of this study. Although no previous reports specify the MIC for AZM treatment, it appears that a 10 μg/mL concentration of AZM results in complete growth inhibition after 24 h of culturing.

3.6. Chlorhexidine and azithromycin co-treatment results in enhanced cytotoxicity in human cancer epithelial cells

The combination was also tested on two colorectal cancer epithelial cell lines, HCT-116 (Fig. 6A) and HT-29 (Fig. 6B). The results show that cytotoxic activity is enhanced when the agents are used together. Notably, the inhibitory concentrations of the agents are significantly higher in the human epithelial cells compared to those used in antibacterial activity analyses. The result also highlights the potential of CHX as a partner in combination with different drug classes for cancer treatment, warranting further investigation.

It appears that the cell's sensitivity to CHX determines the enhanced effectiveness of the AZM and CHX combination. AZM's efficacy may be promoted in bacteria more sensitive to CHX, which is also applicable to the mammalian cancer cells investigated here. Among the two colorectal cancer cell lines, the combination of AZM and CHX showed a higher cytotoxic effect in HCT-116 cells, which are more sensitive to CHX. The greater effectiveness of the combination in cells more responsive to CHX suggests the hypothesis of a CHX-driven mechanism.

Studies on human skin fibroblasts have shown that AZM exhibits cytotoxicity at concentrations of 16 μg/mL and above, and in human skin keratinocytes at concentrations of 64 μg/mL [86]. CHX in a 0.05 % dilution is designed for wound cleansing, and 2 % and 4 % dilutions are designed for surgical skin preparation and as a hand scrub [87]. Therefore, the concentrations used in this study for antibacterial effects for CHX and AZM appear to be safe for mammalian cells, and the effectiveness of the combination warrants investigation *in vivo* and in clinical applications.

4. Discussion

CHX, an antiseptic widely used for about 50 years (both domestically and in healthcare units), is active towards a wide range of Gram-positive and Gram-negative bacteria [88]. Several studies have demonstrated that CHX exhibits greater efficacy than other biocides. Tattawasart et al. compared the activity of cetylpyridinium chloride and CHX against *Pseudomonas* spp., reporting a lower MIC for CHX. Another study involving healthy volunteers highlighted the superior skin disinfection efficacy of CHX over triclosan, recommending its use as an antiseptic prior to surgical procedures [89]. Thus, based on its effectiveness, particularly against *P. aeruginosa*, CHX was combined with AZM in this study. As mentioned above, AZM has modest activity against *P. aeruginosa* and is not considered a highly effective antibiotic against this pathogen, and with long-term low-dose therapy increasing the risk of resistance development. Therefore, CHX was investigated to enhance AZM activity and reduce the antibiotic's MIC.

The results demonstrated here show that the combined application of CHX and AZM significantly inhibits the growth and collagen matrix interaction of the *Pseudomonas aeruginosa* strain PAO1 (isolated from a wound), compared to the individual effects of each agent. Apart from the phenomenon of antibiotic resistance, the use of conventional antibiotics can lead to the extensive release of immunostimulatory bacterial components [90]. While inflammation is a part of the wound healing process, excessive inflammation can result in chronic non-healing wounds,

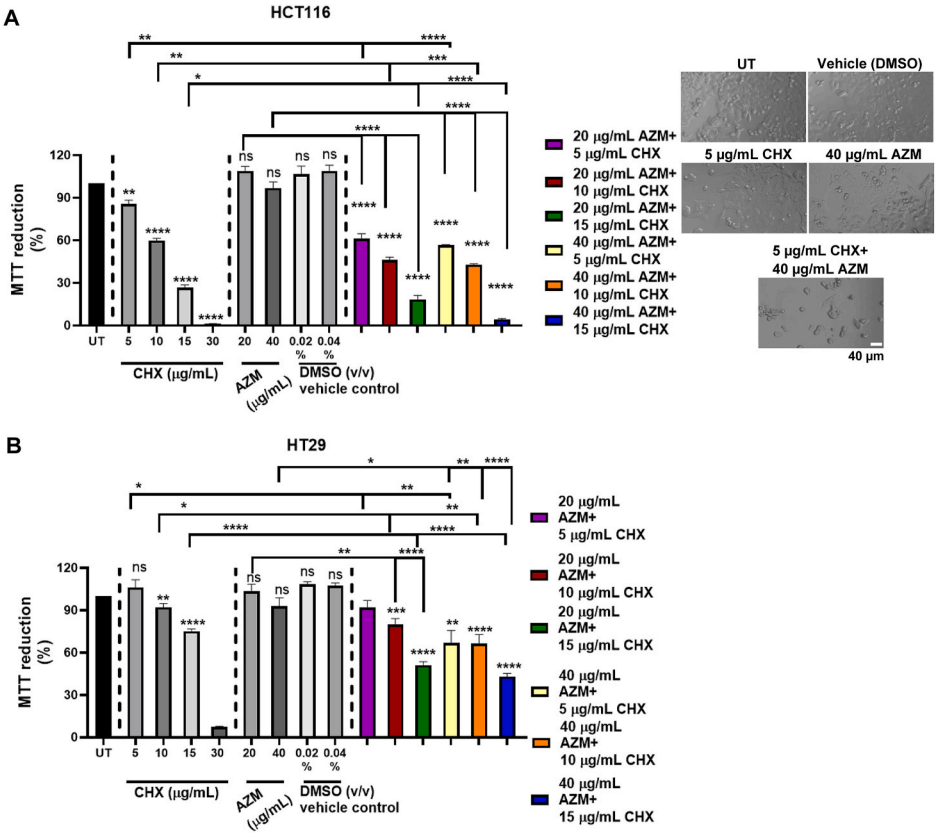

Fig. 6. CHX and AZM show enhanced cytotoxic activity when used in combination in human cancer epithelial cells. After 24 h of incubation, the MTT assay was applied to analyze the cytotoxic effect on A. HCT116 (with photographed cells on the right) and B. HT29 human colorectal cancer cell lines. Cytotoxic activities were evaluated by comparing MTT reduction in the treatment groups with the reduction in untreated control (UT) cells (% inhibition). *t*-test was used for comparisons with the untreated control and between the treatment groups where indicated. Results are presented as mean ± SEM.

preventing progression to the remodeling stage and thereby delaying healing [91] CHX is capable of neutralizing pro-inflammatory cell wall components such as LPS and lipoteichoic acid (LTA) released from bacteria after the bactericidal activity of antibiotics. Thus, when combined with AZM in topical applications, CHX not only has the potential to lower the required antibiotic concentrations but also to neutralize the pro-inflammatory constituents released from bacteria killed by the antibiotic [90]. Additionally, clinical and *in vivo* reports have shown that AZM possesses anti-inflammatory effects and supports the terminal differentiation of keratinocytes in psoriasis against long-term imiquimod use, which is a ligand for Toll-like Receptors TLR7 and TLR8 [92]. Therefore, the combination of AZM and CHX can enhance antibacterial effects in inflamed wounds and has the potential to promote tissue regeneration through immune regulation in inflammatory skin conditions.

To mechanistically explain the observed combinatory effect of CHX and AZM, FTIR spectroscopy was used to identify the bacterial peaks associated with CHX and AZM. This approach shows that while the accumulation of CHX in *P. aeruginosa* does not change with combined application, the bacterial accumulation of AZM increases. Macrolide antibiotics are primarily used for Gram-positive bacterial infections. In Gram-negative bacteria, reduced membrane penetration limits the use of macrolides. However, AZM is more basic in character, resulting in higher permeability across the outer membrane [93]. It is proposed that the electrostatic interaction between AZM and the negatively charged heptose-phosphate region of LPS in the outer membrane structure of Gram-negative bacteria forms a permeability barrier, preventing effective entry of AZM into the cell. AZM has a molecular weight of 749 Da (1.16 nm; $1.3 \times 1.0 \times 0.92$ nm cuboid structure), which is well over the exclusion limit (~600 Da) for passive diffusion across the outer membrane protein (Omp) porin channels located in the outer membrane (OM) of Gram-negative bacteria. However, it enters the cell with the support of its structure, known as "self-promoted uptake." The self-promoted uptake mechanism has been hypothesized as the mechanism for AZM uptake in Gram-negative bacteria. This suggests that after the initial interaction of polycationic antibiotics with divalent cation binding sites on LPS, these compounds competitively displace divalent cations and bind to the LPS, thereby increasing the permeability of the outer membrane to the polycationic antibiotic (hence the name self-promoted uptake) [94,95]. At sub-inhibitory concentrations, cationic CHX molecules can interact with negatively charged LPS regions, effectively "locking" into them. Therefore, the outer membrane of Gram-negative bacteria acts as a permeability barrier for CHX, limiting its antibacterial activity as it cannot reach the cytoplasmic membrane. However, the simultaneous utilization of these two agents in Gram-negative bacteria may transform the drawback of each agent into a benefit. This can be attributed to the possible creation of a hydrophilic interaction zone, which could enhance the entry of AZM into the cell, thereby potentially increasing its effectiveness through CHX action. Alternatively, CHX-dependent perturbations on the outer membrane can affect the structure of outer membrane channel proteins and facilitate the passage of AZM [19].

Studies show that AZM can alter membrane phospholipid organization [96–100]. Most of these studies have investigated the interaction of AZM with model membrane systems. For instance, ^{31}P nuclear magnetic resonance spectroscopy has been used to characterize AZM-induced changes in interactions between neighboring phospholipid head groups. Specifically, membrane-inserted AZM electrostatically binds to anionic phospholipids, reducing the mobility of the phospholipid head groups while increasing the fluidity of the hydrophobic acyl chains. Similarly, atomic force microscopy studies have revealed AZM-induced variations in membrane phospholipid organization. It has been suggested that AZM inserts itself into the bilayer at the interface between the phospholipid head groups and the fatty acyl chains, thereby disrupting the phospholipid organization. Sharifian Gh. et al. used time-resolved second-harmonic light scattering (SHS) to quantify AZM-induced changes in bacterial membrane permeability in colloidal suspensions of living *E. coli*. They showed that immediate treatment with AZM caused no significant changes in membrane permeability. However, prolonged pretreatment with sub-MIC concentrations of AZM resulted in a significant increase in the permeability of both the outer membrane and, through the facilitation of a new transport mechanism, the cytoplasmic membrane of the bacteria. The authors speculated that AZM might be creating well-defined pores across the membrane, but it is also plausible that, similar to the proposed carpet disruption mechanism, AZM induces localized thinning of the membrane. The density of such regions would scale with AZM concentration, allowing for comparatively rapid transport across the membrane, as the authors propose [95]. As presented in this manuscript, the decrease in AZM-dependent ester bond formation in the presence of CHX can support enhanced cellular accumulation of AZM through the phenomenon previously suggested as "localized thinning" [95].

For CHX's interaction and effect on the cell membrane, biguanide groups strongly associate with exposed anionic sites on the cell membrane, as well as the cell wall, particularly acidic phospholipids, and proteins. Binding to these sites displaces wall and membrane-associated divalent cations (Mg^{2+}, Ca^{2+}). The hydrophobic region of CHX, being six carbons long, is somewhat inflexible and incapable of folding sufficiently to interdigitate into the bilayer. Therefore, CHX bridges between pairs of adjacent phospholipid headgroups, each bound to a biguanide moiety, and displaces the associated divalent cations. The distance between phospholipid headgroups in a closely packed monolayer is roughly equivalent to the length of a hexamethylene grouping. Hence, a bisbiguanide would be capable of binding to two adjacent phospholipid headgroups. Such an interaction with the cell membrane reduces membrane fluidity at low concentrations and affects the osmoregulatory and metabolic capabilities of the cell membrane and its enzymes. These effects have been reported as cellular leakage of potassium ions and protons, as well as inhibition of respiration and solute transport. Conversely, at higher concentrations, these interactions are more severe, causing the membrane to adopt a liquid crystalline state, lose its structural integrity, and allow catastrophic leakage of cellular material [88]. Thus, when CHX is used at low concentrations, as in this study, the progressive decrease in the fluidity of the outer phospholipid layer and the creation of hydrophilic domains within the bilayer by CHX can facilitate the passage of AZM from the cellular membrane and enhance its cellular accumulation. It is noteworthy that CHX has been shown to bind LTA similarly to its interaction with LPS [90]. For both Gram-positive and Gram-negative bacteria, particles of approximately 2 nm can pass through the peptidoglycan [101]. Therefore, it can also be speculated that CHX's interaction with peptidoglycan-associated lipids in Gram-positive bacteria (like *S. mutans*) can favor cellular AZM accumulation.

As mentioned, CHX is known to alter the outer membrane charge, which can subsequently affect susceptibility to various antimicrobials [89]. It is also compatible with several commonly used antibiotics [88]. However, in recent decades, numerous reports have highlighted an increase in bacterial resistance to CHX across different species. Studies on *in vitro* CHX-adapted bacteria have revealed cross-resistance between CHX and other antimicrobials, potentially linked to shared resistance mechanisms or the selective pressure caused by the widespread use of CHX, as previously reviewed [89]. This issue is particularly concerning in healthcare settings, where continuous selection pressure from sub-lethal concentrations of CHX could potentially lead to cross-resistance to antibiotics [6], including macrolides [102,103]. Similar caution should be applied to the potential cross-resistance between CHX and other antimicrobials [89], highlighting the importance of recognizing this as a significant concern. Therefore, healthcare providers across various disciplines should be made aware of the potential risks associated with excessive use of CHX in contributing to antimicrobial resistance. To better understand the role of CHX in the selection of multidrug resistance, it is essential to investigate CHX resistance and

cross-resistance not only in the *in vitro* systems, but also in both clinical and environmental isolates.

5. Conclusion

This study highlights the potential of the CHX and AZM combination for topical applications targeting skin infections. Notably, the combination's high efficacy against *S. mutans* suggests the possibility of developing formulations for oral health applications. To advance these prospects, clinical isolates should be tested to evaluate the combination's efficacy. Additionally, investigating other antiseptics for potential synergistic combinations with antibiotics or antimicrobials is warranted. However, it is also important to assess whether such combinations, including CHX with antibiotics, might contribute to resistance development.

Funding information

This work is supported by the Scientific and Technological Research Council of Türkiye (TÜBİTAK), Grant No: 123S179 to STÇ.

Declaration of competing interest

The authors declare that they have no known competing financial interests or personal relationships that could have appeared to influence the work reported in this paper.

Acknowledgments

Acknowledgment is given to the Molecular Biology and Genetics Department and the Biotechnology Application and Research Center of Bilecik Şeyh Edebali University for sharing laboratory facilities. Dr. Dilek Ünal (Bilecik Şeyh Edebali University, Molecular Biology and Genetics Department) is thanked for the fluorescence microscopy facility, Dr. Didem Kart (Hacettepe University, Faculty of Pharmacy), as well as Kübra Demirel, for sharing the strain PAO1, and Dr. Lokman Uzun (Hacettepe University, Chemistry Department) for valuable discussions on the FTIR data. The author sincerely thanks Dr. Mustafa Oğuzhan Çağlayan (Bilecik Şeyh Edebali University, Department of Bioengineering) for his support in analyzing the spectral data and providing feedback on the results. Appreciation is also extended to the members of the STÇ lab for their technical assistance.

Appendix A. Supplementary data

Supplementary data to this article can be found online at https://doi.org/10.1016/j.micpath.2025.107373.

Data availability

Data will be made available on request.

References

[1] M. Tyers, G.D. Wright, Drug combinations: a strategy to extend the life of antibiotics in the 21st century, Nat. Rev. Microbiol. (2019), https://doi.org/10.1038/s41579-018-0141-x.
[2] Y. Zhu, W.E. Huang, Q. Yang, Clinical perspective of antimicrobial resistance in bacteria, Infect. Drug Resist. 15 (2022) 735–746, https://doi.org/10.2147/IDR.S345574.
[3] E. Cacace, V. Kim, V. Varik, M. Knopp, M. Tietgen, A. Brauer-Nikonow, K. Inecik, A. Mateus, A. Milanese, M.T. Mårli, K. Mitosch, J. Selkrig, A.R. Brochado, O. P. Kuipers, M. Kjos, G. Zeller, M.M. Savitski, S. Göttig, W. Huber, A. Typas, Systematic analysis of drug combinations against Gram-positive bacteria, Nat. Microbiol. 8 (2023) 2196–2212, https://doi.org/10.1038/s41564-023-01486-9.
[4] F. Pietsch, G. Heidrich, N. Nordholt, F. Schreiber, Prevalent synergy and antagonism among antibiotics and biocides in Pseudomonas aeruginosa, Front. Microbiol. (2021), https://doi.org/10.3389/fmicb.2020.615618.
[5] E. Elekhnawy, F. Sonbol, A. Abdelaziz, T. Elbanna, Potential impact of biocide adaptation on selection of antibiotic resistance in bacterial isolates, Futur. J. Pharm. Sci. (2020), https://doi.org/10.1186/s43094-020-00119-w.
[6] G. Kampf, Acquired resistance to chlorhexidine – is it time to establish an 'antiseptic stewardship' initiative? J. Hosp. Infect. 94 (2016) 213–227, https://doi.org/10.1016/j.jhin.2016.08.018.
[7] F. Lin, B. Yu, Q. Wang, M. Yuan, B. Ling, Combination inhibition activity of chlorhexidine and antibiotics on multidrug-resistant Acinetobacter baumannii in vitro, BMC Infect. Dis. 21 (2021) 266, https://doi.org/10.1186/s12879-021-05963-6.
[8] B.S.J. Gregorchuk, S.L. Reimer, C.J. Slipski, K.A. Milner, S.L. Hiebert, D. R. Beniac, T.F. Booth, G.G. Zhanel, D.C. Bay, Applying fluorescent dye assays to discriminate Escherichia coli chlorhexidine resistance phenotypes from porin and mlaA deletions and efflux pumps, Sci. Rep. 12 (2022) 12149, https://doi.org/10.1038/s41598-022-15775-6.
[9] K.S. Lim, P.C.A. Kam, Chlorhexidine - pharmacology and clinical applications, Anaesth. Intensive Care (2008), https://doi.org/10.1177/0310057x0803600404.
[10] F. Cieplik, N.S. Jakubovics, W. Buchalla, T. Maisch, E. Hellwig, A. Al-Ahmad, Resistance toward chlorhexidine in oral bacteria-is there cause for concern? Front. Microbiol. (2019) https://doi.org/10.3389/fmicb.2019.00587.
[11] M.J. Parnham, V.E. Haber, E.J. Giamarellos-Bourboulis, G. Perletti, G. M. Verleden, R. Vos, Azithromycin: mechanisms of action and their relevance for clinical applications, Pharmacol. Ther. (2014), https://doi.org/10.1016/j.pharmthera.2014.03.003.
[12] A.G. Leroy, J. Caillon, N. Caroff, A. Broquet, S. Corvec, K. Asehnoune, A. Roquilly, L. Crémet, Could azithromycin Be part of Pseudomonas aeruginosa acute pneumonia treatment? Front. Microbiol. (2021) https://doi.org/10.3389/fmicb.2021.642541.
[13] M. Heidary, A. Ebrahimi Samangani, A. Kargari, A. Kiani Nejad, I. Yashmi, M. Motahar, E. Taki, S. Khoshnood, Mechanism of action, resistance, synergism, and clinical implications of azithromycin, J. Clin. Lab. Anal. 36 (2022) 1–16, https://doi.org/10.1002/jcla.24427.
[14] Y. Hooda, A.M. Tanmoy, M.S.I. Sajib, S. Saha, Mass azithromycin administration: considerations in an increasingly resistant world, BMJ Glob. Health (2020), https://doi.org/10.1136/bmjgh-2020-002446.
[15] M.H. Mustafa, S. Khandekar, M.M. Tunney, J.S. Elborn, B.C. Kahl, O. Denis, P. Plésiat, H. Traore, P.M. Tulkens, F. Vanderbist, F. Van Bambeke, Acquired resistance to macrolides in Pseudomonas aeruginosa from cystic fibrosis patients, Eur. Respir. J. (2017), https://doi.org/10.1183/13993003.01847-2016.
[16] R. Raizman, W. Little, A.C. Smith, Rapid diagnosis of Pseudomonas aeruginosa in wounds with point-of-care fluorescence imaing, Diagnostics (2021), https://doi.org/10.3390/diagnostics11020280.
[17] C.R. Belanger, A.H.Y. Lee, D. Pletzer, B.K. Dhillon, R. Falsafi, R.E.W. Hancock, Identification of novel targets of azithromycin activity against Pseudomonas aeruginosa grown in physiologically relevant media, Proc. Natl. Acad. Sci. U. S. A 117 (2020) 33519–33529, https://doi.org/10.1073/pnas.2007626117.
[18] L. Goltermann, K.L. Andersen, H.K. Johansen, S. Molin, R. La Rosa, Macrolide therapy in Pseudomonas aeruginosa infections causes uL4 ribosomal protein mutations leading to high-level resistance, Clin. Microbiol. Infect. 28 (2022) 1594–1601, https://doi.org/10.1016/j.cmi.2022.08.003.
[19] G. Samgane, S. Karaçam, S. Tunçer Çağlayan, Unveiling the synergistic potency of chlorhexidine and azithromycin in combined action, Naunyn-Schmiedebergs Arch Pharmacol (2024), https://doi.org/10.1007/s00210-024-03010-0.
[20] K. Doğan, S. Tunçer Çağlayan, Capsaicin shows species and strain-specific activity: investigation of the antibacterial effects on the oral pathogen Streptococcus mutans and the oral probiotics Streptococcus salivarius M18 and K12, Hacettepe J. Biol. Chem. 52 (2024) 11–19, https://doi.org/10.15671/hjbc.1337284.
[21] E. Werner, F. Roe, A. Bugnicourt, M.J. Franklin, A. Heydorn, S. Molin, B. Pitts, P. S. Stewart, Stratified growth in Pseudomonas aeruginosa biofilms, Appl. Environ. Microbiol. (2004), https://doi.org/10.1128/AEM.70.10.6188-6196.2004.
[22] L. Barnes V, D.M. Heithoff, S.P. Mahan, J.K. House, M.J. Mahan, Antimicrobial susceptibility testing to evaluate minimum inhibitory concentration values of clinically relevant antibiotics, STAR Protoc. (2023), https://doi.org/10.1016/j.xpro.2023.102512.
[23] X. Liu, R. Liu, R. Zhao, J. Wang, Y. Cheng, Q. Liu, Y. Wang, S. Yang, Synergistic interaction between paired combinations of natural antimicrobials against poultry-borne pathogens, Front. Microbiol. (2022), https://doi.org/10.3389/fmicb.2022.811784.
[24] T. Ding, Z. Guo, L. Fang, W. Guo, Y. Yang, Y. Li, X. Li, L. He, Synergistic antibacterial effects of closantel and its enantiomers in combination with colistin against multidrug resistant gram-negative bacteria, Front. Microbiol. 15 (2024), https://doi.org/10.3389/fmicb.2024.1374910.
[25] D.J. Noel, C.W. Keevil, S.A. Wilks, Synergism versus additivity: defining the interactions between common disinfectants, mBio 12 (2021), https://doi.org/10.1128/mBio.02281-21.
[26] C. Zhou, Q. Wang, L. Jin, R. Wang, Y. Yin, S. Sun, J. Zhang, H. Wang, In vitro synergistic activity of antimicrobial combinations against blaKPC and blaNDM-producing enterobacterales with blaIMP or mcr genes, Front. Microbiol. (2020), https://doi.org/10.3389/fmicb.2020.533209.
[27] T.C. Chou, The combination index (CI < 1) as the definition of synergism and of synergy claims, Synergy 7 (2018) 49–50, https://doi.org/10.1016/j.synres.2018.04.001.
[28] D. Duarte, N. Vale, Evaluation of synergism in drug combinations and reference models for future orientations in oncology, Curr. Res. Pharmacol. Drug Discov. (2022), https://doi.org/10.1016/j.crphar.2022.100110.

[29] S. Karaçam, S. Tunçer, Lyophilized cell-free supernatants of the oral probiotics Streptococcus salivarius M18 and Streptococcus salivarius K12 show promises for milk safety, Lett. Appl. Microbiol. 76 (2023) 1–10, https://doi.org/10.1093/lambio/ovac034.

[30] S. Karaçam, S. Tunçer, Exploiting the acidic extracellular pH: evaluation of Streptococcus salivarius M18 postbiotics to target cancer cells, probiotics antimicrob, Proteins 14 (2022) 995–1011, https://doi.org/10.1007/s12602-021-09806-3.

[31] S. Tunçer, R. Gurbanov, Non-growth inhibitory doses of dimethyl sulfoxide alter gene expression and epigenetic pattern of bacteria, Appl. Microbiol. Biotechnol. (2022) 299–312, https://doi.org/10.1007/s00253-022-12296-0.

[32] S. Tunçer, S. Karaçam, Cell-free supernatant of Streptococcus salivarius M18 impairs the pathogenic properties of Pseudomonas aeruginosa and Klebsiella pneumonia, Arch. Microbiol. (2020), https://doi.org/10.1007/s00203-020-02005-8.

[33] T.F. Bahamondez-Canas, L.A. Heersema, H.D.C. Smyth, Current status of in vitro models and assays for susceptibility testing for wound biofilm infections, Biomedicines (2019), https://doi.org/10.3390/biomedicines7020034.

[34] L. Corte, D.C. Pierantoni, C. Tascini, L. Roscini, G. Cardinali, Biofilm specific activity: a measure to quantify microbial biofilm, Microorganisms (2019), https://doi.org/10.3390/microorganisms7030073.

[35] M. Barsainya, D.P. Singh, Green synthesis of zinc oxide nanoparticles by Pseudomonas aeruginosa and their broad-spectrum antimicrobial effects, J. Pure Appl. Microbiol. (2018), https://doi.org/10.22207/JPAM.12.4.50.

[36] B.L. Price, A.M. Lovering, F.L. Bowling, C.B. Dobson, Development of a novel collagen wound model to simulate the activity and distribution of antimicrobials in soft tissue during diabetic foot infection, antimicrob, Agents Chemother. 60 (2016) 6880–6889, https://doi.org/10.1128/AAC.01064-16.

[37] M. Werthén, L. Henriksson, P.Ø. Jensen, C. Sternberg, M. Givskov, T. Bjarnsholt, An in vitro model of bacterial infections in wounds and other soft tissues, APMIS 118 (2010) 156–164, https://doi.org/10.1111/j.1600-0463.2009.02580.x.

[38] S. Tunçer, A.G.A.G. Keşküş, M. Çolakoğlu, I. Çimen, C. Yener, Ö. Konu, S. Banerjee, 15-Lipoxygenase-1 re-expression in colorectal cancer alters endothelial cell features through enhanced expression of TSP-1 and ICAM-1, Cell, Signal 39 (2017) 44–54, https://doi.org/10.1016/j.cellsig.2017.07.022.

[39] R. Gurbanov, S. Tunçer, The Use of Fourier-Transform Infrared Spectroscopy to Determine Potential Starch-Based Prebiotics, 4, 2021, pp. 22–30, https://doi.org/10.18016/ksutarimdoga.vi.742250.

[40] D.K. Agustika, I. Mercuriani, C.W. Purnomo, S. Hartono, K. Triyana, D.D. Iliescu, M.S. Leeson, Fourier transform infrared spectrum pre-processing technique selection for detecting PYLCV-infected chilli plants, Spectrochim. Acta Part A Mol. Biomol. Spectrosc. 278 (2022) 121339, https://doi.org/10.1016/j.saa.2022.121339.

[41] J.K. Wallis, V. Krömker, J.H. Paduch, Biofilm challenge: lactic acid bacteria isolated from bovine udders versus staphylococci, Foods (2019), https://doi.org/10.3390/foods8020079.

[42] N.C. Cady, K.A. McKean, J. Behnke, R. Kubec, A.P. Mosier, S.H. Kasper, D.S. Burz, R.A. Musah, Inhibition of biofilm formation, quorum sensing and infection in Pseudomonas aeruginosa by natural products-inspired organosulfur compounds, PLoS One 7 (2012) e38492, https://doi.org/10.1371/journal.pone.0038492.

[43] K.P. Rumbaugh, Biofilms in the ICU, southwest respir, Crit. Care Chronicles 2 (2014) 15–18, https://doi.org/10.12746/swrccc2013.0206.067.

[44] K. Sauer, P. Stoodley, D.M. Goeres, L. Hall-Stoodley, M. Burmølle, P.S. Stewart, T. Bjarnsholt, The biofilm life cycle: expanding the conceptual model of biofilm formation, Nat. Rev. Microbiol. 20 (2022) 608–620, https://doi.org/10.1038/s41579-022-00767-0.

[45] Y. Li, O.E. Petrova, S. Su, G.W. Lau, W. Panmanee, R. Na, D.J. Hassett, D. G. Davies, K. Sauer, BdlA, DipA and induced dispersion contribute to acute virulence and chronic persistence of Pseudomonas aeruginosa, PLoS Pathog. 10 (2014) e1004168, https://doi.org/10.1371/journal.ppat.1004168.

[46] D.A. Amly, P. Hajardhini, A.L. Jonarta, H.D.K. Yulianto, H. Susilowati, Enhancement of pyocyanin production by subinhibitory concentration of royal jelly in Pseudomonas aeruginosa, F1000Research 10 (2021) 14, https://doi.org/10.12688/f1000research.27915.4.

[47] L.Y. Chimi, M. Noubom, B.N. Bisso, G.S. Singor Njateng, J.P. Dzoyem, Biofilm Formation, pyocyanin production, and antibiotic resistance profile of Pseudomonas aeruginosa isolates from wounds, Internet J. Microbiol. 2024 (2024) 1–10. https://www.hindawi.com/journals/ijmicro/2024/1207536/.

[48] T. Gonçalves, U. Vasconcelos, Colour me blue: the history and the biotechnological potential of pyocyanin, Molecules (2021), https://doi.org/10.3390/molecules26040927.

[49] A.F. Bettencourt, J. Costa, I.A.C. Ribeiro, L. Gonçalves, M.T. Arias-Moliz, J. R. Dias, M. Franco, N.M. Alves, J. Portugal, C.B. Neves, Development of a chlorhexidine delivery system based on dental reline acrylic resins, Int. J. Pharm. 631 (2023) 122470, https://doi.org/10.1016/j.ijpharm.2022.122470.

[50] K. Garala, P. Joshi, J. Patel, A. Ramkishan, M. Shah, Formulation and evaluation of periodontal in situ gel, Int. J. Pharm. Investig (2013), https://doi.org/10.4103/2230-973x.108961.

[51] T.T.N. Huynh, K. Padois, F. Sonvico, A. Rossi, F. Zani, F. Pirot, J. Doury, F. Falson, Characterization of a polyurethane-based controlled release system for local delivery of chlorhexidine diacetate, Eur. J. Pharm. Biopharm. 74 (2010) 255–264, https://doi.org/10.1016/j.ejpb.2009.11.002.

[52] B.M. Priyadarshini, S.T. Selvan, K. Narayanan, A.S. Fawzy, Characterization of chlorhexidine-loaded calcium-hydroxide microparticles as a potential dental pulp-capping material, Bioengineering (2017), https://doi.org/10.3390/bioengineering4030059.

[53] T. Rema, J.R. Lawrence, J.J. Dynes, A.P. Hitchcock, D.R. Korber, Microscopic and spectroscopic analyses of chlorhexidine tolerance in delftia acidovorans biofilms, Antimicrob. Agents Chemother. 58 (2014) 5673–5686, https://doi.org/10.1128/AAC.02984-14.

[54] R.K. Kotecha, S. Bhadra, K.S. Rajesh, Formulation & process development of azithromycin ophthalmic nanosuspension, Int. J. Pharm. Pharmaceut. Sci. 5 (2013) 490–497.

[55] Q.G. Liao, L.F. Hu, L.G. Luo, A chitosan-polypyrrole@Fe3O4 nanocomposite for magnetic solid-phase extraction of macrolides from swine urine samples, Anal. Methods (2015), https://doi.org/10.1039/c4ay02907k.

[56] N.F. Robaina, C.E.R. de Paula, D.M. Brum, M. de la Guardia, S. Garrigues, R. J. Cassella, Novel approach for the determination of azithromycin in pharmaceutical formulations by Fourier transform infrared spectroscopy in film-through transmission mode, Microchem. J. (2013), https://doi.org/10.1016/j.microc.2013.04.015.

[57] Y. Liu, H.-J. Kim, Fourier transform infrared spectroscopy (FT-IR) and simple algorithm analysis for rapid and non-destructive assessment of developmental cotton fibers, Sensors 17 (2017) 1469, https://doi.org/10.3390/s17071469.

[58] P.B. Kasangana, T. Stevanovic, Studies of pentacyclic triterpenoids structures and antidiabetic properties of Myrianthus genus, Stud. Nat. Prod. Chem. (2021), https://doi.org/10.1016/B978-0-12-819485-0.00014-1.

[59] M.K. Mishra, Fourier transform infrared spectrophotometry studies of chromium trioxide-phthalic acid complexes, Chem. Sci. Trans. 5 (2016), https://doi.org/10.7598/cst2016.1260.

[60] S.C. Ray, C.W. Pao, H.M. Tsai, J.W. Chiou, W.F. Pong, M.H. Tsai, T.I.T. Okpalugo, P. Papakonstantinou, T.W. Pi, Enhancement of sp3-bonding in high-bias-voltage grown diamond-like carbon thin films studied by x-rayabsorption and photoemission spectroscopy, J. Phys. Condens. Matter (2007), https://doi.org/10.1088/0953-8984/19/17/176204.

[61] Y.A. Abdu, F.C. Hawthorne, M.E. Varela, Infrared spectroscopy of carbonaceous-chondrite inclusions in the kapoeta meteorite: discovery of nanodiamonds with new spectral features and astrophysical implications, Astrophys. J. Lett. (2018), https://doi.org/10.3847/2041-8213/aab433.

[62] L. Robinet, S. Heu-Thao, M. Radepont, C. Bonnot-Diconne, Non-invasive analysis of gilt leather gold varnish and protective layer by infrared reflection-absorption spectroscopy, Vib. Spectrosc. (2020), https://doi.org/10.1016/j.vibspec.2020.103133.

[63] B. Hofko, M.Z. Alavi, H. Grothe, D. Jones, J. Harvey, Repeatability and sensitivity of FTIR ATR spectral analysis methods for bituminous binders, Mater. Struct. Constr. (2017), https://doi.org/10.1617/s11527-017-1059-x.

[64] M.A. Mallah, S.T.H. Sherazi, S.A. Mahesar, A. Rauf, Assessment of Azithromycin in Pharmaceutical Formulation by Fourier-Transform Infrared (FT- IR) Transmission Spectroscopy, 12, 2011, pp. 61–67. file:///C:/Users/Sinem/Downloads/Assessment_of_Azithromycin_in_Pharmaceutical_Formu.pdf.

[65] A.-M. Udrea, A. Dinache, J.-M. Pagès, R.A. Pirvulescu, Quinazoline derivatives designed as efflux pump inhibitors: molecular modeling and spectroscopic studies, Molecules 26 (2021) 2374, https://doi.org/10.3390/molecules26082374.

[66] L. Elmlund, P. Söderberg, S. Suriyanarayanan, I.A. Nicholls, A phage display screening derived peptide with affinity for the adeninyl moiety, Biosensors (2014), https://doi.org/10.3390/bios4020137.

[67] G. Fischer, The Chemistry of pyrido[1,2-a]azepines and their hydro derivatives. https://doi.org/10.1016/B978-0-12-386011-8.00002-2, 2011.

[68] M.R. Bindhu, M. Umadevi, Green synthesized gold nanoparticles as a probe for the detection of Fe3+ ions in water, J. Cluster Sci. (2014), https://doi.org/10.1007/s10876-013-0679-8.

[69] P. Karimineghlani, P.K. Neghlani, A. Azadmehr, Optimization of lead ions adsorption on hydrolyzed polyacrylonitrile fibers using central composite design, Desalination Water Treat. (2017), https://doi.org/10.5004/dwt.2017.21063.

[70] K.I. Hadjiivanov, D.A. Panayotov, M.Y. Mihaylov, E.Z. Ivanova, K.K. Chakarova, S.M. Andonova, N.L. Drenchev, Power of infrared and Raman spectroscopies to characterize metal-organic frameworks and investigate their interaction with guest molecules, Chem. Rev. 121 (2021) 1286–1424, https://doi.org/10.1021/acs.chemrev.0c00487.

[71] A. Elena, I. Gozescu, A. Dabici, P. Sfirloaga, Z. Szabadai, Organic compounds FT-IR spectroscopy, in: Macro to Nano Spectrosc, InTech, 2012, https://doi.org/10.5772/50183.

[72] E. Jaradat, A. Meziane, D.A. Lamprou, Conventional vs PEGylated loaded liposomal formulations by microfluidics for delivering hydrophilic chemotherapy, Int. J. Pharm. 655 (2024) 124077, https://doi.org/10.1016/j.ijpharm.2024.124077.

[73] J. Kong, S. Yu, Fourier transform infrared spectroscopic analysis of protein secondary structures, Acta Biochim. Biophys. Sin. (2007), https://doi.org/10.1111/j.1745-7270.2007.00320.x.

[74] K.B. Bec, R. Wieczorek, B. Lydzba-Kopczyzska, J.P. Hawranek, Analysis of infrared spectra of neat liquid N-methylpyrrole, Acta Phys. Pol. A (2013), https://doi.org/10.12693/APhysPolA.124.115.

[75] S. Tunçer Çağlayan, R. Gurbanov, Modulation of bacterial membranes and cellular macromolecules by dimethyl sulfoxide: a dose-dependent study providing novel insights, Int. J. Biol. Macromol. 267 (2024) 131581, https://doi.org/10.1016/j.ijbiomac.2024.131581.

[76] F.G. Adebawo, V. Naithani, H. Sadeghifar, D. Tilotta, L.A. Lucia, H. Jameel, O. Y. Ogunsanwo, Morphological and interfacial properties of chemically-modified tropical hardwood, RSC Adv. 6 (2016) 6571–6576, https://doi.org/10.1039/C5RA19409A.

[77] J. Meneghel, S. Passot, F. Jamme, S. Lefrançois, P. Lieben, P. Dumas, F. Fonseca, FTIR micro-spectroscopy using synchrotron-based and thermal source-based radiation for probing live bacteria, Anal. Bioanal. Chem. (2020), https://doi.org/10.1007/s00216-020-02835-x.
[78] A. Pistiki, A. Ramoji, O. Ryabchykov, D. Thomas-Rüddel, A.T. Press, O. Makarewicz, E.J. Giamarellos-Bourboulis, M. Bauer, T. Bocklitz, J. Popp, U. Neugebauer, Biochemical analysis of leukocytes after in vitro and in vivo activation with bacterial and fungal pathogens using Raman spectroscopy, Int. J. Mol. Sci. 22 (2021) 10481, https://doi.org/10.3390/ijms221910481.
[79] T. Chakkumpulakkal Puthan Veettil, D. Alves, J. Vongsvivut, R.L. Sparrow, B. R. Wood, G. Garnier, Characterization of freeze-dried oxidized human red blood cells for pre-transfusion testing by synchrotron FTIR microspectroscopy live-cell analysis, Analyst 148 (2023) 1595–1602, https://doi.org/10.1039/D2AN02001G.
[80] A. De la Rosa-Tilapa, A. Maceda, T. Terrazas, Characterization of biominerals in cacteae species by FTIR, Crystals (2020), https://doi.org/10.3390/cryst10060432.
[81] N. Dave, V.A. Lórenz-Fonfría, J. Villaverde, R. Lemonnier, G. Leblanc, E. Padrós, Study of amide-proton exchange of Escherichia coli melibiose permease by attenuated total reflection-Fourier transform infrared spectroscopy: evidence of structure modulation by substrate binding, J. Biol. Chem. 277 (2002) 3380–3387, https://doi.org/10.1074/jbc.M105466200.
[82] C.M. Baronio, A. Barth, The amide i spectrum of proteins - optimization of transition dipole coupling parameters using density functional theory calculations, J. Phys. Chem. B (2020), https://doi.org/10.1021/acs.jpcb.9b11793.
[83] N. Vázquez-Laslop, A.S. Mankin, How macrolide antibiotics work, Trends Biochem. Sci. (2018), https://doi.org/10.1016/j.tibs.2018.06.011.
[84] G. Donadio, M.G. Chini, V. Parisi, F. Mensitieri, N. Malafronte, G. Bifulco, A. Bisio, N. De Tommasi, A. Bader, Diterpenoid constituents of psiadia punctulata and evaluation of their antimicrobial activity, J. Nat. Prod. (2022), https://doi.org/10.1021/acs.jnatprod.1c01093.
[85] S.V. Shah, C.M. Badakar, S.M. Hugar, S. Hallikerimath, K. Gowtham, M. V. Mundada, Antimicrobial efficacy of chlorhexidine and herbal mouth rinse on salivary Streptococcus mutans in children with mixed dentition: a randomized crossover study, Int. J. Clin. Pediatr. Dent. (2022), https://doi.org/10.5005/jp-journals-10005-2348.
[86] Z. Rukavina, M. Šegvić Klarić, J. Filipović-Grčić, J. Lovrić, Ž. Vanić, Azithromycin-loaded liposomes for enhanced topical treatment of methicillin-resistant Staphyloccocus aureus (MRSA) infections, Int. J. Pharm. 553 (2018) 109–119, https://doi.org/10.1016/j.ijpharm.2018.10.024.
[87] Wound healing and management node group, evidence summary: wound management -chlorhexidine, wound pract, Res. 25 (2017) 49–52.
[88] P. Gilbert, L.E. Moore, Cationic antiseptics: diversity of action under a common epithet, J. Appl. Microbiol. 99 (2005) 703–715, https://doi.org/10.1111/j.1365-2672.2005.02664.x.
[89] H.M. Abbood, K. Hijazi, I.M. Gould, Chlorhexidine resistance or cross-resistance, that is the question, Antibiotics (2023), https://doi.org/10.3390/antibiotics12050798.
[90] M. Zorko, R. Jerala, Alexidine and chlorhexidine bind to lipopolysaccharide and lipoteichoic acid and prevent cell activation by antibiotics, J. Antimicrob. Chemother. 62 (2008) 730–737, https://doi.org/10.1093/jac/dkn270.
[91] Z. Wang, F. Qi, H. Luo, G. Xu, D. Wang, Inflammatory microenvironment of skin wounds, Front. Immunol. 13 (2022), https://doi.org/10.3389/fimmu.2022.789274.
[92] S.-W. Huang, J.-J. Shieh, The antibiotic azithromycin improves the severity of imiquimod-induced psoriasis-like skin inflammation in mice, J. Dermatol. Sci. (2016), https://doi.org/10.1016/j.jdermsci.2016.08.210.
[93] C. Gomes, L. Ruiz-Roldán, J. Mateu, T.J. Ochoa, J. Ruiz, Azithromycin resistance levels and mechanisms in Escherichia coli, Sci. Rep. 9 (2019) 6089, https://doi.org/10.1038/s41598-019-42423-3.
[94] S. Farmer, Z. Li, R.E.W.W. Hancock, Influence of outer membrane mutations on susceptibility of escherichia coli to the dibasic macrolide azithromycin, J. Antimicrob. Chemother. 29 (1992) 27–33, https://doi.org/10.1093/jac/29.1.27.
[95] M.S. Gh, M.J. Wilhelm, H.L. Dai, Azithromycin-induced changes to bacterial membrane properties monitored in vitro by second-harmonic light scattering, ACS Med. Chem. Lett. (2018), https://doi.org/10.1021/acsmedchemlett.7b00499.
[96] J.P. Montenez, F. Van Bambeke, J. Piret, R. Brasseur, P.M. Tulkens, M.P. Mingeot-Leclercq, Interactions of macrolide antibiotics (erythromycin A, roxithromycin, erythromycylamine [dirithromycin], and azithromycin) with phospholipids: computer-aided conformational analysis and studies on acellular and cell culture models, Toxicol. Appl. Pharmacol. (1999), https://doi.org/10.1006/taap.1999.8632.
[97] D. Tyteca, A. Schanck, Y.F. Dufrêne, M. Deleu, P.J. Courtoy, P.M. Tulkens, M. P. Mingeot-Leclercq, The macrolide antibiotic azithromycin interacts with lipids and affects membrane organization and fluidity: studies on Langmuir-blodgett monolayers, liposomes and J774 macrophages, J. Membr. Biol. (2003), https://doi.org/10.1007/s00232-002-1076-7.
[98] A. Berquand, M.-P. Mingeot-Leclercq, Y.F. Dufrêne, Real-time imaging of drug–membrane interactions by atomic force microscopy, Biochim. Biophys. Acta Biomembr. 1664 (2004) 198–205, https://doi.org/10.1016/j.bbamem.2004.05.010.
[99] N. Fa, L. Lins, P.J. Courtoy, Y. Dufrêne, P. Van Der Smissen, R. Brasseur, D. Tyteca, M.-P. Mingeot-Leclercq, Decrease of elastic moduli of DOPC bilayers induced by a macrolide antibiotic, azithromycin, Biochim. Biophys. Acta Biomembr. 1768 (2007) 1830–1838, https://doi.org/10.1016/j.bbamem.2007.04.013.
[100] N. Fa, S. Ronkart, A. Schanck, M. Deleu, A. Gaigneaux, E. Goormaghtigh, M.-P. Mingeot-Leclercq, Effect of the antibiotic azithromycin on thermotropic behavior of DOPC or DPPC bilayers, Chem. Phys. Lipids 144 (2006) 108–116, https://doi.org/10.1016/j.chemphyslip.2006.08.002.
[101] P. Demchick, A.L. Koch, The permeability of the wall fabric of Escherichia coli and Bacillus subtilis, J. Bacteriol. 178 (1996) 768–773, https://doi.org/10.1128/jb.178.3.768-773.1996.
[102] R. Früh, A. Anderson, F. Cieplik, E. Hellwig, A. Wittmer, K. Vach, A. Al-Ahmad, Antibiotic resistance of selected bacteria after treatment of the supragingival biofilm with subinhibitory chlorhexidine concentrations, Antibiotics (2022), https://doi.org/10.3390/antibiotics11101420.
[103] J.G.E. Laumen, C. Van Dijck, S.S. Manoharan-Basil, S. Abdellati, I. De Baetselier, V. Cuylaerts, T. De Block, D. Van den Bossche, B.B. Xavier, S. Malhotra-Kumar, C. Kenyon, Sub-inhibitory concentrations of chlorhexidine induce resistance to chlorhexidine and decrease antibiotic susceptibility in Neisseria gonorrhoeae, Front. Microbiol. (2021), https://doi.org/10.3389/fmicb.2021.776909.